View metadata, citation and similar papers at core.ac.uk

brought to you by CORE

provided by Helsingin yliopiston digitaalinen arkisto

M.Sc. Thesis
Meteorology

Wind drift of snowfall between the radar volume and ground

Tuomo Lauri

February 8, 2010

Supervisors: M.Sc. Jarmo Koistinen (FMI), Dr. Dmitri Moisseev

Reviewers: Prof. Hannu Savijärvi, M.Sc. Jarmo Koistinen (FMI)

UNIVERSITY OF HELSINKI
DEPARTMENT OF PHYSICS

P.O. BOX 64 (Gustaf Hällströmin katu 2)
FIN-00014 University of Helsinki

Contents

1 Introduction

Weather radars are useful tools for measuring precipitation for a variety of purposes. Radars combine high spatial coverage with temporal and spatial resolution, producing frequent observations over large areas. Radar observations can be used in precipitation nowcasting and gathering of high resolution precipitation statistics as well as in indirect applications such as detection of supercooled water, hail occurrence and observation of severe weather such as tornadoes (Battan 1973).

Radar reflectivity factor data is rarely used in its "raw" form, but is instead filtered and manipulated to make the quantitative precipitation estimation (QPE) more accurate. Depending on the application, several correction schemes are applied to the data, including the removal of non-meteorological targets, correction for vertical profile of reflectivity (VPR), attenuation correction etc. Correction schemes significantly improve data quality and thus radar performance at ground level QPE.

Although the radar rainfall estimates are operationally obtained with a variety of algorithms, a correction for wind drift of precipitation between the radar contributing volume aloft and ground has received much less attention. In operational radar systems it is assumed that hydrometeors fall vertically to the ground and thus, a radar measurement is representative for the geographical location below the measurement. However, e.g. at 200 km distance from the radar the radar beam is approximately 3 km above the ground. With a horizontal wind of $10\frac{m}{s}$ and fall speed of $1\frac{m}{s}$, the measured hydrometeors will be advected 30 kilometers from the radar measuring location during their fall time.

This study evaluates the errors in radar-based precipitation estimation at ground level caused by wind drift as well as examines in which conditions the effect is most prevalent. Previous studies have shown (e.g. (Collier 1999)) that errors caused by wind drift are likely to be largest when high resolution measurements from areas of steep rainfall gradient are required. This suggests that in terms of rainfall, nowcasting of intense rain events seems a likely application for drift correction.

In addition to rainfall products, visibility estimates would also benefit from wind drift correction. In colder climates such as that of Finland, among the most important causes of poor visibility is snowfall. As the terminal velocity of snow particles is typically much smaller than that of rain, snow is prone to drift considerable distances. It is unlikely that any visibility product for high latitudes will be successful without wind drift correction of radar measurements. For these reasons this work

mainly concerns wind drift in the case of snowfall and evaluation of wind drift in rainfall was omitted as melting layer effects complicate radar observations and therefore frustrate analysis. Previous studies have also shown that wind drift of rainfall is unimportant for all but the highest of precipitation grid resolutions (Fabry et al. 1994).

In this work typical wind drift distances in Finnish conditions are computed using sounding data. Precipitation phase is estimated from the soundings in order to assess its effect on the drift distance statistics.

The effect of wind drift on radar measurements is evaluated by applying a trajectory-based correction scheme to radar PPI images. The effects of trajectory-correction are evaluated as a function of range from radar and precipitation accumulation interval. The significance of correction to precipitation events with different spatial structures is also briefly explored.

An attempt to estimate the relative error of precipitation wind drift to QPE in the case of snowfall is made. The magnitude of drift error is determined by using known drifting distances and the spatial structure of the precipitation field. This error is compared to other known sources of error in order to evaluate the contribution of wind drift to QPE uncertainty.

In chapter 2 a brief introduction to the basics of precipitation measurements using radar and rain gauges is given. The effect of wind drift on radar observations is analysed in chapter 3. The methodology to determine the wind drift and the estimation of its statistical distribution are assessed in chapters 4 and 5, respectively. In Chapter 6 the trajectory determination is applied to transferring the PPI images to the ground level. The contribution of wind drift to the overall uncertainty of radar observations is analysed in Chapter 7. The results of this work are summarized and discussed in Chapter 8 with concluding remarks and recommendations. Appendices A and B present figures illustrating wind drift statistics and comparison of corrected and uncorrected radar reflectivity time series, respectively.

2 Scientific background

2.1 Basics of precipitation measurement by rain gauges and radars

Traditionally, rainfall amounts are estimated using weather stations equipped with weighing rain gauges. Since gauges measure the rainfall *in situ* they are considered the closest representation of the real rain (and are often called "the ground truth"). Gauges can measure rainfall intensity with a maximum temporal resolution of approximately 1 minute. The maximum resolution in rainfall amount is generally in the order of 0.1 mm. Therefore rain gauges are accurate enough to detect most types of rainfall, save for the very lightest drizzle (Goodison et al. 1997).

The main problem in using rain gauges is that while their temporal resolution is often sufficient, their spatial resolution is not. As gauge measurements are point observations, one has to have a distribution of gauges in order to describe the spatial structure of the rain. The required spatial resolution (or gauge density) depends on the situation. Available rain gauge networks rarely have the spatial resolution required to study anything but the largest precipitating structures like fronts or stratiform rain. In addition, the gauges are mostly located near urban areas. This makes the gauge network easier to maintain and enhances resolution in populated (and hence important) areas. The drawback is low coverage in rural areas. If such areas are large (as in Finnish Lapland) the low coverage can result in bias in rainfall statistics and difficulties in hydrological forecasting and other public services. The coverage issue is even more severe in coastal areas, as measurements from sea are scarce. Expanding the rain gauge network is costly, considering that each weather station requires maintenance and above all infrastructure to operate (Battan 1973).

To combat these limitations, weather radars are used to complement rain gauge networks. A radar can measure rainfall within 250 kilometer radius from the radar with a typical spatial resolution of about 1 km^2. Separate scans of the entire area of coverage can be made once every 5 minutes, giving the radar superior spatial and temporal coverage as well as resolution. Radars can be positioned so that they cover areas inaccessible to other instruments, thus providing often unique information. A single radar can cover large swaths of water or wilderness, which would be impossible or extremely difficult to cover with *in situ* measurements. Radars are also able to provide short-term rainfall forecasts, which are important in prediction of small-scale

hazards, such as local flooding due to intense rain (Battan 1973).

2.2 Uncertainties inherent in precipitation measurements

2.2.1 Radar reflectivity factor and Doppler velocity

Radars use microwave radiation to infer properties of weather targets. Radar measures by sending a pulse of radiation, usually around 2 μs long, and listening for the backscattering echoes. From these echoes, the targets' range and direction can be measured as well as a number of target parameters, the number of which depends on the features of the radar. The most common scanning strategy is simply to rotate the antenna with constant angular velocity and elevation angle, producing a PPI (Plan Position Indicator) data file. The PPI image displays radar returns as a function of range and azimuth (Battan 1973).

A typical modern monostatic radar consists of a parabolic transmitter and receiver antenna producing a pencil-shaped beam. The width of the beam depends on the radius of the antenna dish and the wavelength used, but is generally approximately 1°. The on-beam resolution is determined by the pulse length with a typical value of 500 meters. For a radar with these specifications, this translates to a spatial resolution of about 0.5 km^2 at 50 kilometer distance and 1.7 km^2 at 200 kilometer distance. The volume from which the backscattered radiation originates at a given instant is called the contributing volume.

Each radar measurement is in reality a set of independent pulses from which the parameters are calculated statistically. This improves the reliability of radar measurements.

In its basic form a radar measures only the power of the radiation scattered back by the targets. An equation is therefore needed to relate the power to target characteristics. This equation is called the radar equation, and can be expressed in a simplified form as follows (Austin 1987):

$$\bar{P}_r = \frac{CkZ}{r^2} \tag{2.1}$$

Here $\bar{P}_r$ is the average received power, C is a constant containing parameters related to the radar, k is two-way signal attenuation along the path of beam propagation and r is range from radar. The most important parameter however is Z or the radar reflectivity factor. When the radar wavelength is much larger than the

circumference of the scatterers (Rayleigh scattering domain), Z can expressed as a function of scatterer properties, namely (Battan 1973):

$$Z = \sum_{V_c} D_i^6 \tag{2.2}$$

where $\sum$ is the number of the sixth powers of scatterer diameters (D) in the contributing volume. Since Z can have a wide range of values (due to the D^6 - dependency), a logarithmic derivative of it is commonly used:

$$dBZ = 10 \log_{10} \frac{Z}{1 \frac{mm^6}{m^3}}$$

The scatterers are usually assumed to be water in the form of raindrops or cloud droplets, and therefore the radar signal processors use the dielectric constant (not explicitly shown in Eq. 2.1) of liquid water to compute Z. However, microwaves are scattered by a variety of targets, such as birds, insects, areas of gradient in air refractive index, tall masts etc. Even in the absence of non-meteorological targets the backscattered signal can (and frequently will in high latitudes) originate from snow. Problems introduced by snow are discussed in more detail in section 2.4. When measuring targets that are not liquid water, the measured Z is strictly speaking Z_e, meaning (water) equivalent radar reflectivity factor (Battan 1973).

The phase shift between the transmitted and received radar signals can be used to estimate the target's velocity. Radar signals are electromagnetic waves, and therefore experience Doppler shift in their frequency when scattered by a moving target. The velocity of the target can be calculated from the associated phase difference.

The phase difference is however a cyclic measure and therefore inherently ambiguous. For this reason the measured differences are assumed to be "along the shortest path", meaning all phase differences are taken to be between $]-180°, 180°]$, or in terms of velocity, $\left]-\frac{\lambda}{4T}, \frac{\lambda}{4T}\right]$. Here λ is the radar wavelength and T the sampling interval. This means that any phase shift (and therefore velocity) beyond this interval is incorrectly represented. The maximum unambiguous velocity is called the Nyquist velocity and is a function of the pulse repetition frequency PRF (rays per second) and wavelength of the radar (Battan 1973):

$$V_N = \pm \frac{\lambda}{4} PRF \tag{2.3}$$

It should be noted however, that only the radial velocity component, parallel to the radar beam, is measured. For this and other reasons, the true three-dimensional wind field cannot be calculated using observations from a single radar. With additional constraints (such as linearity of the wind field and small vertical motions), the local wind field can be estimated using different methods. Perhaps most importantly, the vertical wind profile can be estimated using a method called Volume Velocity Processing (VVP) (Waldteufel and Corbin 1979).

As each radar measurement is in reality an average over several independent pulses, the velocity distribution in each volume can be estimated. From this distribution, the mean radial velocity (Doppler velocity) can be calculated, as well as the standard deviation of the distribution. The standard deviation is called the velocity spectrum width (or simply spectrum width), and is a measure of turbulence, wind shear and antenna rotation within the measuring volume (Battan 1973).

2.3 Issues in radar derived rain rate

As mentioned earlier, Z is related to the amount of water in the contributing volume. This relation is ambiguous, however, since different drop size distributions (DSD) can result in an equal value of Z, as can be seen from its definition (Eq. 2.2). This means that the exact water content or rain rate in the contributing volume cannot be deduced from the Z value alone. Unless the DSD is known, Z can only be interpreted as the relative rainfall intensity within the same DSD domain. This is perhaps the most fundamental challenge in using radar to estimate rain.

The problem can be partially circumvented by measuring DSDs in different rainfall types and constructing what are called Z(R) relations for the rainfall types in question. The relationships are in the form of $Z = aR^b$, where a and b are constants depending on the DSD (and therefore rainfall type). They are calculated directly from the measured DSDs or estimated by measuring rain with both radar and rain gauges, and comparing reflectivities and gauge measurements. The latter method, however, is sensitive to errors in both measurement systems i.e. coefficients a and b may then contain other influencing factors than those originating from the DSD alone (Battan 1973).

Similar relationships can be calculated also for solid state precipitation. These are called $Z_e(S)$ relationships, but are less useful than Z(R) relationships for a number of reasons, some of which are discussed in section 2.4.

Even when using these relationships, in order to quantitatively measure precipitation, its type and structure has to be known *a priori*, which limits the usefulness of those relationships. There are many relationships in literature for different geographical areas, different precipitation types, different radars etc. For further discussion on Z(R) relationships see e.g. Battan (1973). Quite often it is not known how much the given relations contain effects of system errors in addition to the natural variation of the precipitation.

The measuring geometry of the radar must also be taken into account when estimating rainfall. Curvature of the Earth and atmospheric refraction usually cause the radar beam to deflect upwards relative to the ground. The exact height of the radar beam depends on the range from the radar and the vertical structure of the atmospheric refractive index. When conditions for anomalous propagation exist (such as surface temperature inversion), the path of the radar beam can be very complex. In normal conditions, and when approximate results are sufficient, the radar beam height can be expressed as (Battan 1973):

$$h(r) = h_0 + r\sin(\alpha) + \frac{r^2}{2R_e} \tag{2.4}$$

Here h_0 is the radar altitude, r is range from the radar along ground, α is the radar beam elevation angle and $R_e = \gamma R$ where R is the radius of Earth. The coefficient γ is introduced to take atmospheric refraction into account. Refraction in standard atmosphere translates to $\gamma \approx \frac{4}{3}$. In total, typical atmospheric conditions cause the beam to ascend as if the Earth radius was one third larger with no refraction.

This upward deflection has two consequences. Firstly, the radar does not measure rainfall at ground level. Depending on the distance from radar, the beam height can be anything from hundreds of meters to few kilometers. The rain measured at a certain height can undergo growth or dissipation processes which cause differences between the measured rainfall intensity at ground level and aloft. For this reason, a vertical profile of reflectivity (VPR) correction must be applied. This means extrapolating the measured Z to the ground level using estimated VPR below each lowest elevation radar measurement.

The second consequence is wind drift. The rainfall measured by radar is generally assumed to fall vertically to the same horizontal location where the corresponding reflectivity was measured, either immediately or after some assumed fall time. While this certainly is the case when winds are negligible, or the radar beam is very near

to the ground, a significant non-zero wind field will advect the rain downwind. The extent of the drift depends on the radar measuring height (and therefore distance from the radar), the prevailing winds and the fall speed of precipitation. The effect of wind drift on radar measurement geometry is illustrated in Fig. 2.1.

The two problems caused by beam height are not independent. VPR correction schemes assume that reflectivity profiles are indeed vertical. In reality, the profiles should be evaluated along the paths of falling precipitation, or fall streaks (see section 3.1) . When strong winds are present, these paths are not vertical but slanted, which introduces error in a VPR correction (unless the VPR shape is horizontally homogeneous).

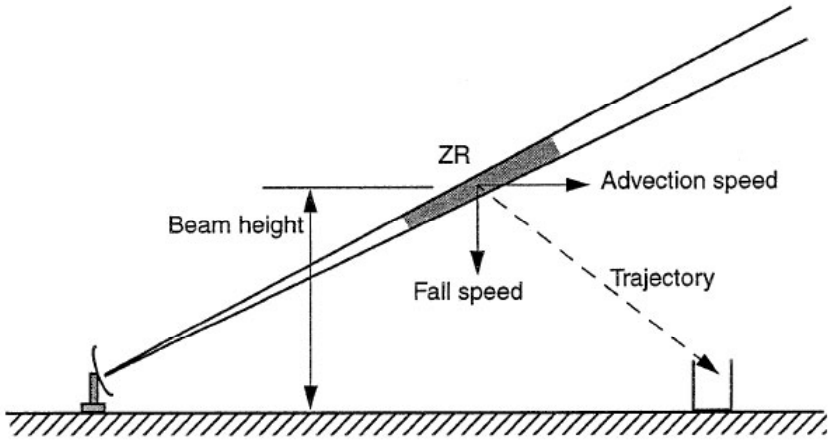

Figure 2.1 *Schematic diagram showing measuring geometry of a radar - rain gauge pair. Advection with wind causes the gauge to measure precipitation not originating from immediately above. Figure adapted from Rasmussen et al. (2003).*

2.4 Errors in snowfall measurements

Snowfall is generally more difficult to measure than rain for all instruments, both *in situ* and with remote sensing such as radar.

As radar rain estimates are based primarily on reflectivity, the measurements are sensitive to particle sizes and electromagnetic properties. Let us first consider liquid rain in the contributing volume. Surface tension tends to keep raindrops roughly spherical (or ellipsoid) during their fall. Moreover, the density of water is practically constant in atmospheric conditions. This means that the relation between drop size and its water content can be rather accurately established. This reduces the problem

of volume water content to merely estimation of the DSD (although this problem is by no means simple). Rain intensity estimation requires additional knowledge in the form of raindrop fall speeds, but they can be related to drop size, and therefore DSD (see section 3.3). Estimation of snowfall is however a much more complex problem.

In contrast to liquid water, snow is far from homogeneous. Depending on the conditions in which the solid precipitation formed, it can take the form of dendrites, columns, plates, graupel, hail or some combination thereof. Each form has distinct properties, such as density and shape. Therefore the water content of a snowflake is not a simple function of its size, even if the "size" can be meaningfully defined. From this it follows that there is no simple relation between Z_e and the associated snow or water content in the contributing volume. In the case of nonspherical scatterers, Z_e depends on the orientation and shape of the scattering particles. For this reason one needs additional constraints (such as randomly distributed orientations) to solve the scattering properties of irregular particles. However, it has been shown (Smith 1984) that for small snowflakes (compared to the radar wavelength) the irregularities in snowflake shape are irrelevant and the flakes can be handled as spheres of equal mass. Thus, similarly to rainfall, water equivalent snowfall rate (S in $\frac{mm}{hr}$) can be estimated from the measured radar reflectivity factor as a $S(Z_e)$ relation, provided that the particle size distribution (PSD) is known or can be estimated (e.g. Sekhon and Srivastava (1971)).

The presence of hail introduces another problem that is exclusive for solid state precipitation. Unlike raindrops and most snowflakes, hailstones can grow significantly large compared to the typical weather radar wavelengths. The wavelength of a C - band radar is approximately 5 cm, and hailstones of similar size occur occasionally. For these large particles, the Rayleigh scattering approximation is not valid. This causes precipitation rates to become unrealistically high in the presence of hail (assuming Rayleigh - approximation is valid), a phenomenon called "hail contamination".

It should also be noted that reflectivities between raindrops and snow are not comparable, as snow and water have different dielectric constants and therefore different scattering properties even assuming they are of similar shape (Smith 1984).

2.4.1 Snow and rain gauges

Rain gauges have their own sources of error when measuring snow. Weighing gauges typically measure snow by melting the catch at regular intervals and measuring the

water equivalent. This removes the problem of differing densities, as all types of snow are reduced to water and snowfall intensities to corresponding rainfall intensities. The problem in this approach is that while it makes different snowfall types comparable, the different properties of snowflakes are lost. The water equivalent is not very useful to most applications, as it cannot be immediately related to more meaningful quantities, such as snow depth or density.

A more severe problem in gauge measurements of snow is the snowflakes' low fall speed and small mass compared to raindrops. These cause snow to be highly susceptible to small scale turbulence, which is a severe problem with gauge measurements of snow. Even when properly positioned, the gauge itself produces turbulence that affects the paths of falling snowflakes (usually guiding the snowflakes over or around the gauge) and causes errors in snowfall measurements. Moreover, measured snowfall can result from snow already fallen to the ground elsewhere but lifted back into the air by wind. These problems can be partially solved using wind shields in conjunction with the gauges. Shields attempt to mitigate the effects of turbulence and make the measurements more representative. There is however a number of different wind shield types in use and the optimal shielding configuration depends on the properties of the gauge and its surroundings.

Systematic errors caused by wind and turbulence increase with wind speed. In WMO Solid Precipitation Measurement Intercomparison (Goodison et al. 1997) the errors caused by wind and turbulence on gauge measurements of snow were evaluated. In the study several types of rain gauge wind shields were compared against the Double Fence Intercomparison Reference (DFIR), which is a Tretyakov -shielded rain gauge equipped with a wind shield and two octagonal outer fences of different heights. This setup is currently considered to give the best estimate for ground precipitation. The bias of a gauge is described by its catch ratio, which is the gauge measurement (in this case the Finnish standard, a Tretyakov - shielded gauge) divided by the corresponding DFIR measurement. Fig. 2.2 shows the catch ratio of Tretyakov gauges as a function of wind speed at gauge level. The catch ratio (and therefore accuracy) decreases significantly when even weak winds are present. The catch ratio depends also on the air temperature, but this effect was deemed comparatively small for snow events, although becoming more important in wet snow (Goodison et al. 1997). The complete formula for Tretyakov-shielded gauge catch ratio in snow is

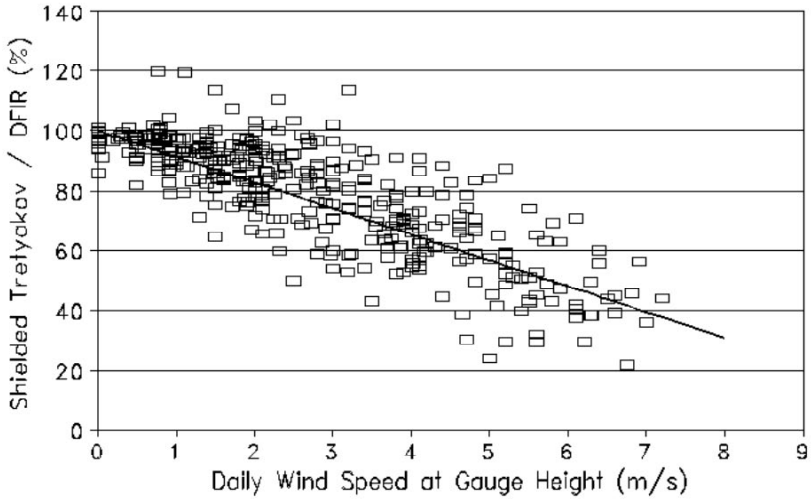

Figure 2.2 *Comparison of catch ratio between a shielded Tretyakov gauge and DFIR as a function of wind speed at gauge level. Underestimation bias increases rapidly with wind speed. The curve is computed from snow events with a maximum daily temperature of -10 °C. Figure adapted from Goodison et al. (1997).*

$$CR = 103.10 - 8.67W + 0.30T_{max} \quad (\text{n} = 394,\ \text{r} = 0.66) \tag{2.5}$$

Here CR is abbreviation of catch ratio, W_s is mean wind speed and T_{max} is daily maximum temperature in degrees Celsius. From Eq. 2.5 one can see that 10 degree difference in the maximum air temperature results in 3% change in catch ratio, whereas $1\frac{m}{s}$ difference in wind speed results in approximately 9% change.

3 The effect of wind drift on radar observations

3.1 Effect of wind shear on drifting

As mentioned earlier, wind drift is defined as the amount of horizontal displacement of precipitation between the radar contributing volume and the corresponding location on the ground. There are two ways to approach the problem. Consider a precipitating cloud measured at a certain height from the ground. Hydrometeors falling from the cloud are subjected to wind drift and are displaced horizontally. If there is no vertical wind shear, i.e. the wind field is constant during the fall, the hydrometeors move at the same horizontal speed as the precipitating cloud and there is no apparent drift (relative to the measured cloud). In this case, the point where the precipitation reaches ground is always directly below the cloud. It would be tempting to deduce that wind drift is trivial in such a case, but during the precipitation fall time the cloud may have undergone processes that have changed its properties, such as the DSD. For this reason the drops measured on the ground do not necessarily represent the cloud immediately above.

A constant wind field is rare in nature, however. In the atmospheric boundary layer the wind profile is commonly approximated by the Ekman-Taylor spiral, meaning wind gets weaker and turns to the left towards the ground. Using this model requires information about the terrain and atmospheric static stability, and therefore is rarely useful in wind drift studies. A simpler model of constant vertical wind shear is generally used in the absence of better estimations. In this simplification, the wind profile is a linear function of height, from zero at ground level to V_{max} at some reference height.

With a constant vertical wind shear, hydrometeors higher from the ground move at faster speeds than those below, resulting in a curved trajectory. A straightforward mathematical analysis shows that the trajectories are parabolic in respect to height (see e.g. Gunn and Marshall (1955)). Because of this non-linearity, the location where precipitation reaches the ground is in fact never directly below the originating cloud. Moreover, there are two possible locations for the precipitation at ground level depending on how we define the problem, apparent in Fig. 3.1. If we are interested in where the precipitation will fall from the measured cloud, we must follow the trajectories of individual hydrometeors, denoted with dashed lines in the figure. On the other hand, if we want to know where the precipitation is falling

at the instant of the measurement, we must follow what are called "fall streaks", denoted with solid lines. These lines represent a snapshot of the hydrometeors falling from the same part of the cloud (or generating element within large scale precipitation) at a certain instant. The difference between the two is that while trajectories are paths of single hydrometeors as they fall, fall streaks are formed by connecting hydrometeors released from the same origin at different times. If we follow the nomenclature introduced by Mittermaier et al. (2004), the cases involving trajectories and fall streaks are called "prognostic" and "diagnostic", respectively. The separation of trajectories and fall streaks depends on the choice of coordinate system. Relative to the cloud the two concepts appear as one.

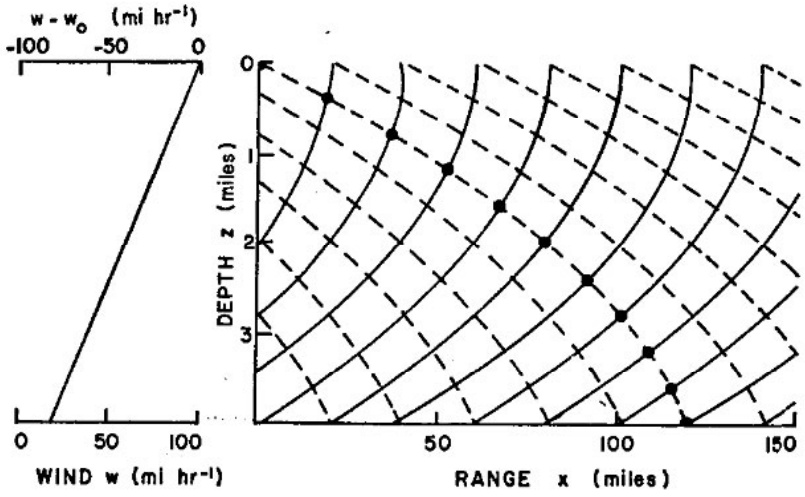

Figure 3.1 *A linear wind profile with the corresponding trajectories and fall streaks. Hydrometeors are released at regular intervals from a point source. Dashed lines represent trajectories of individual hydrometeors. Solid lines are fall streaks, representing the currently falling hydrometeors at each instant. The hydrometeor fall speed is assumed to be 1 m/s. Figure adapted from Marshall (1953).*

Fall streaks are most prominent when there is an isolated source of rain, such as a lone but intense cumulonimbus cloud. Occasionally streaks can be seen even with the naked eye. When there is a sufficiently strong wind the streaks can be seen bending backwards as they approach ground, very much like in the simplified model. A light rain event with visible fall streaks is presented in Fig. 3.2.

Now suppose we have a rain gauge in the path of the precipitating cloud and we intend to compare radar and gauge measurements. The radar is therefore measuring exactly above the gauge. Because of the wind shear, the surface precipitation follows

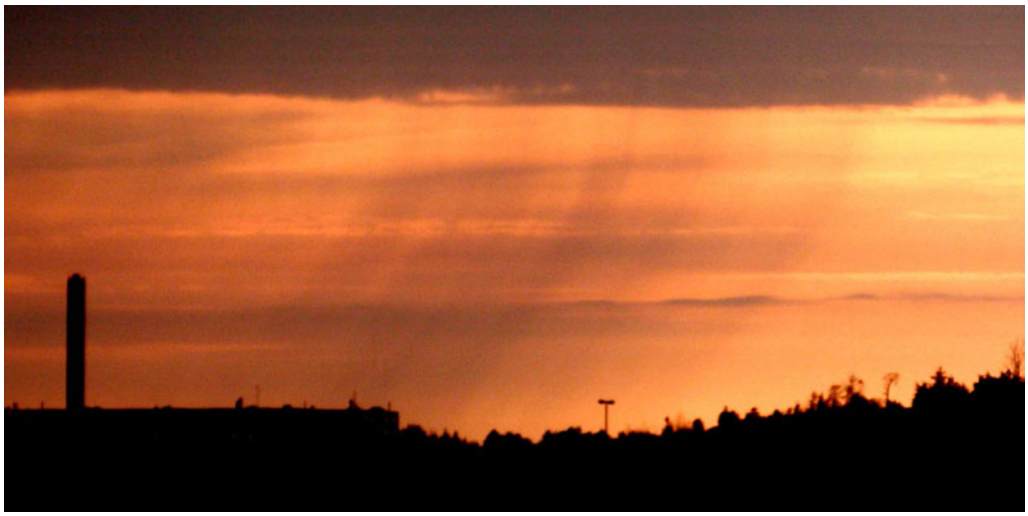

Figure 3.2 *Fall streaks photographed at Viikki, Helsinki on 13. June 2009. Rainfall is light with low terminal fall speed, producing notable streaks. Note the nearly parabolic streak shape.*

the cloud with a certain lag, which depends on hydrometeor fall speed, wind speeds and fall height. If we measure rain in the leading edge of the cloud with a radar, there isn't necessarily any precipitation on the ground immediately below. For this reason we have two conflicting measurements, one from the radar which sees precipitation, and other from the gauge which sees nothing. This "edge effect" is caused by the vertical wind shear and finite hydrometeor fall time. Even when the rain has reached the gauge, the radar measurement directly above the gauge does not represent the precipitation measured at ground level which leads to discrepancies, for example when estimating Z(R) - relationships.

3.2 Dependence on temporal and spatial resolution of observations

Let us assume we want to measure cumulative precipitation at a certain point on the ground, using radar and a rain gauge in the same manner as in section 3.1. For illustration purposes, consider the following simplified model of an approaching rain cloud. We have a precipitating cloud at certain height, moving at a constant speed. The precipitation field is taken to be spatially uniform. For simplicity's sake, the wind is taken to be non-existent below the cloud, producing fall streaks that are linear but slanted backwards. Furthermore, let us assume that both the

radar and the gauge measure rain perfectly, meaning that all differences between the two measurements are solely caused by the wind drift of precipitation. As previously explained, there will be an initial discrepancy in the measured cumulative precipitation between the two instruments, the amount of which depends on the magnitude of the drift. This discrepancy becomes relatively smaller with time, once the precipitation has reached the gauge. This is essentially the edge effect mentioned in section 3.1, and is demonstrated in Fig. 3.3.

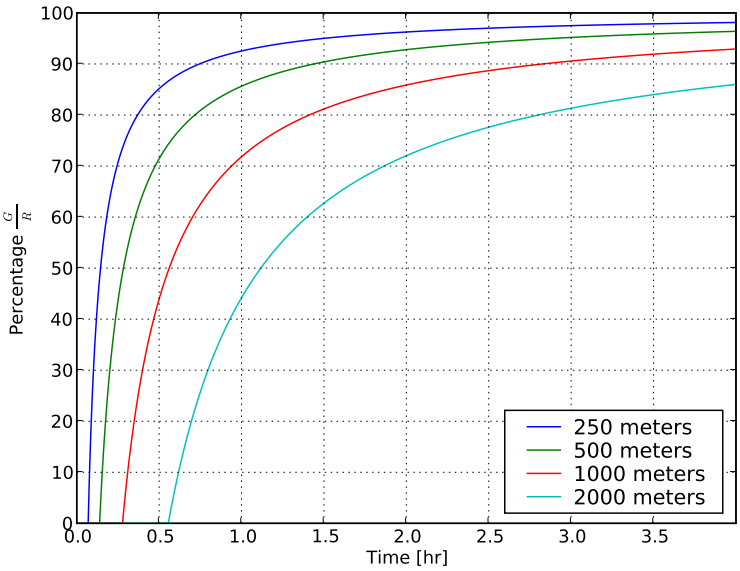

Figure 3.3 *The relative difference between cumulative rain gauge and radar measurements from the same horizontal location as a function of time. The lag in precipitation fall streaks reaching the ground causes the different measured accumulations. Different lines represent different radar measuring heights with greater height producing larger wind drift. Wind speed is assumed to be 10 m/s at generating level height and zero elsewhere. Hydrometeors are taken to be snow with a fall speed of 1 m/s.*

The presented model is extremely simple, but clearly demonstrates the fact that the errors caused by wind drift depend on the time spans in question. While instantaneous measurements would certainly benefit from wind drift correction, the benefit is not at all clear when considering longer time scales. In the example in Fig. 3.3, after approximately three hours the ground measurements corresponding the three lowest fall heights all account for 90% of the radar-measured precipitation. On the other hand, it takes from about 15 to 90 minutes for the ground-level measurements

with lowest three fall heights to accumulate 80% of the radar precipitation. This points to the fact that while nowcasting applications such as local visibility products could be improved with wind drift correction, products covering longer time spans such as daily precipitation statistics would benefit little.

It would seem natural that the errors caused by wind drift increase when the spatial resolution of the rainfall measurements is increased. For end-user products the rainfall fields are given in grids of varying spatial resolution. For a given wind field and radar measuring height, one can calculate the mean drifting distance, or characteristic drift, for a given area and hydrometeor type. If the characteristic drift is much smaller than the grid resolution, drift is unlikely to change the resulting precipitation field. On the other hand, if the characteristic drift is larger than grid resolution, a grid square will receive very little of the precipitation above, which suggests errors in radar estimated rainfall amounts.

Collier (1999) studied radar rainfall data with different grid resolutions. It was found out, that while reducing the grid square size from 5 km to 2 km did increase accuracy, further reduction to ≈ 1 km resulted in no improvement. This "accuracy saturation" when increasing the grid resolution was attributed to wind drift. Similar observations were made by Lack and Fox (2007). Harrold et al. (1975) concluded that radar measurements over a point are least accurate, in contrast to rain gauges which provide an accurate point measurement.

In addition to the resolution of observations, the structure of the precipitation field itself is a factor when determining the effect of wind drift. The amount of horizontal variability in the precipitation field is directly proportional to the error due to wind drift. Areas of high precipitation intensity gradient are most prone to errors due to wind drift. On the other hand, an ideal homogeneous precipitation field is error-free, no matter how strong the winds are. Large scale stratiform rain is therefore least affected by drift, whereas in convective precipitation the effect is most pronounced. Despite this, even stratiform precipitation is not without edges and internal structure. Even if precipitation is stratiform at ground level, it is in most cases produced by distinct generating cells aloft (Marshall 1953). For this reason, the problem of wind drift is present in practically all precipitation types.

3.3 Wind drift and hydrometeor fall speed

The amount of wind drift in precipitation is sensitive to hydrometeor terminal fall speed. In general case, fall speed of hydrometeors relative to the ground depends on hydrometeor phase, particle size, surrounding air density and possible updrafts. There is no analytical solution in the general case, although formulas that apply for a certain hydrometeor type and diameter interval have been developed. For example, the following formulae were presented by Atlas et al. (1973):

$$\begin{aligned} V_{rain}(D)[\tfrac{cm}{s}] &= 965 - 1030e^{-6D}, \quad 0.06cm < D < 0.58cm \\ V_{snow}(D)[\tfrac{cm}{s}] &= 207D^{0.31} \end{aligned} \tag{3.1}$$

From Eq. 3.1 it can be seen that the raindrop fall speed has an asymptote at large drop sizes, while for snow the fall speed increases monotonically. The main reason is that raindrops have an upper bound in drop size because surface tension becomes relatively weaker with increasing drop diameter. This causes drops to split into smaller ones after a certain size. In contrast, ice particles can grow very large, owing their maximum practical size to atmospheric conditions rather than particles themselves, thanks to their solid nature.

Even if the relation between the hydrometeor size and the fall speed is known (or assumed), the DSD of the precipitation has to be taken into account when dealing with real precipitation. As hydrometeor sizes follow a certain distribution, there is also a distribution of fall speeds within the precipitation. Lower speed enables hydrometeors to spend more time airborne and therefore advect further in respect to the originating cloud. For this reason trajectories and fall streaks are not identical even within a single generating element and fall streaks tend to fan out as they approach ground. This effect is called "drop sorting" because, at ground level, larger raindrops that fall faster appear at the front edge of a moving fall streak, after which the average drop size decreases. Drop sorting is illustrated in Fig. 3.4.

Although snowflakes can become larger than raindrops in terms of particle diameter, the fall speed of snow is rather low and roughly independent of flake size (see Fig. 4.2), as seen from Eq. 3.1 (as $V_{snow} \propto \sqrt[3]{D_{snow}}$). This is why there is less variation in snowflake fall speeds compared to raindrops. In conclusion, size sorting is less pronounced in snowfall although the wind drift distances are longer than with rainfall.

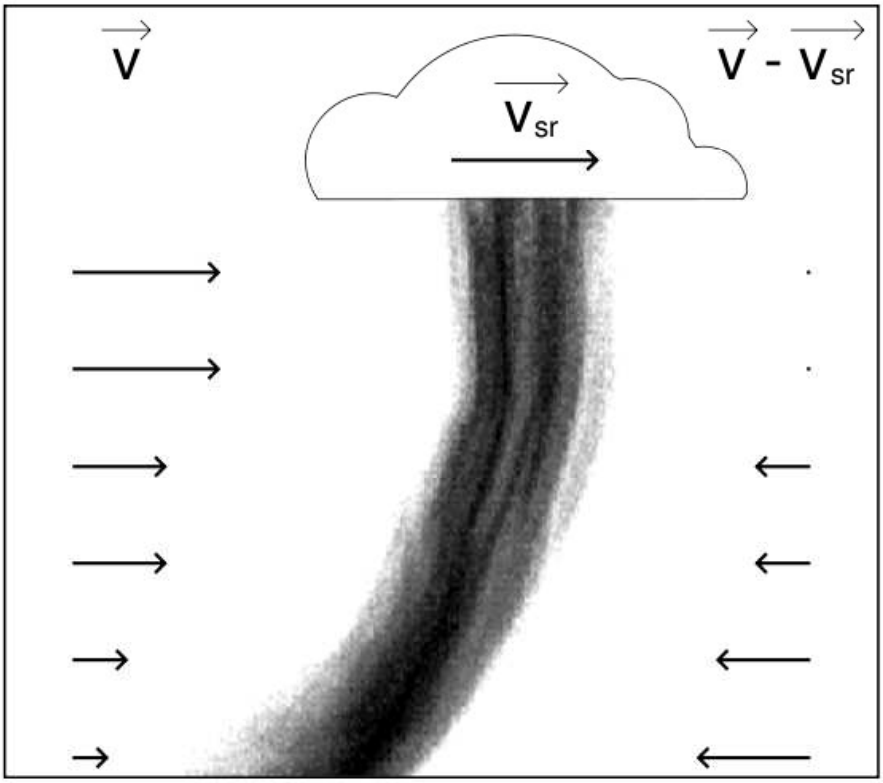

Figure 3.4 *Trail measured by a vertically pointing radar with prevailing winds $\vec{V}$ and with the speed of the generating cell $\vec{V_{sr}}$. Wind shear causes the parabolic fall streak shape. Note the intense core of large raindrops (near left side of the fall streak at cloud level and right side near ground) which is less affected by wind shear. Figure adapted from Fabry (1993).*

The degree of riming (and therefore density) of solid precipitation also affects its fall speed. Rimed particles like graupel suffer less air resistance relative to their mass and have higher fall speeds than aggregate snow.

4 Methodology to determine hydrometeor trajectories

4.1 Determining hydrometeor fall speeds

Fall speed is of utmost importance when estimating precipitation drift distances. There are essentially two ways to determine fall speeds, either measure them directly or estimate the PSD of the precipitation and apply a known fall speed formula to yield the velocity distribution.

The PSD approach is difficult for a number of reasons. Measuring PSD directly requires specialized equipment, namely disdrometers. There are two major disdrometer types, impact and imaging. Impact disdrometers measure drop sizes by measuring the vertical momentum of the falling particle and converting it into particle size. Imaging disdrometers essentially take photographs of falling precipitation and particle sizes are determined from the images.

Impact disdrometers are unable to measure snow because of the low fall speed and ambiguous size - fall speed relation. Imaging disdrometers are able to differentiate between different precipitation types, but these instruments are uncommon and data for this study was not readily available. Even for imaging disdrometers the PSD in snowfall is difficult to measure, since they essentially see a 2D shadow of the particle instead of the full 3D structure (Löffler-Mang and Joss 2000). This poses a serious problem when the measured particles are highly irregular, as aggregated snowflakes often are.

Fall speed formulas are defined relative to the air surrounding the falling particle. In order to estimate the fall speed relative to the ground (or effective fall speed), updraft velocities should be accounted for. The magnitude of updrafts varies greatly from several meters per second in precipitating cumulus clouds to centimeters per second in stratiform precipitation. The problem is that vertical air motion is a very difficult quantity to measure or even estimate indirectly.

In this study a vertically measuring Doppler radar was used to measure the particle fall velocities. This method was chosen for a number of reasons. With a Doppler radar, both the Doppler velocity and velocity spectrum width can be measured as a function of height. From this it follows that measurements from summertime precipitation produce velocities for both rain and snow, simplifying the analysis. Furthermore, the measured Doppler velocities include possible air

motion and therefore represent the effective fall speeds relative to the ground. The spectrum width is an indicator of scatter in the fall speeds and can be used in error estimation.

A possible downside is that the Doppler velocities are reflectivity weighed averages over particles in the contributing volume. Therefore large particles contribute more to the velocity spectrum and the Doppler velocity is larger than the arithmetic mean of the velocities.

To determine fall speeds for rain and snow, velocity data from 6 was used days from the Järvenpää (vertically looking) Doppler radar, operated by University of Helsinki. The data consisted of 6318 individual beams in eight data sets with a combined duration of approximately 24 hours. Each data set was measured during stratiform summertime precipitation, and included the Doppler velocity and spectrum width as a function of time and height. An example of a time - height indicator scan produced by the radar is presented in Fig. 4.1.

To differentiate between rain and snow, and to get deeper insight on how the fall speed behaves as a function of temperature, a vertical temperature profile was extracted from a nearby sounding for each data set. Soundings were made at Jokioinen observatory, approximately 100 kilometers from the radar site. For each dataset, the most representative sounding was chosen. The majority of the radar measurements took place within 4 hours from the corresponding sounding. The soundings should therefore represent the vertical temperature structure at the radar site fairly well.

To relate the measured fall speed and spectrum width with temperature, the temperature profiles were used to interpolate temperatures to the radar measurement levels. Then each level was averaged to acquire the mean fall speed for the temperature in question. The same treatise was applied to spectrum width data. This was done to all data sets separately, yielding eight different fall speed and spectrum width profiles. In Fig 4.2 the measured fall speeds and spectrum widths for each case are plotted against the extracted temperatures at the radar measurement levels.

Fig 4.2 shows that the fall speed behaviour of snow is nearly similar in each case. In all cases the fall speed of snow is nearly independent of temperature (and therefore height). There are, however, quite large differences in the snow flake size distributions between the cases, as indicated by the differing fall speeds in the rain below the freezing level. This supports the argument that the fall speed of snow has very little variation from one precipitation event to another. The rather low and

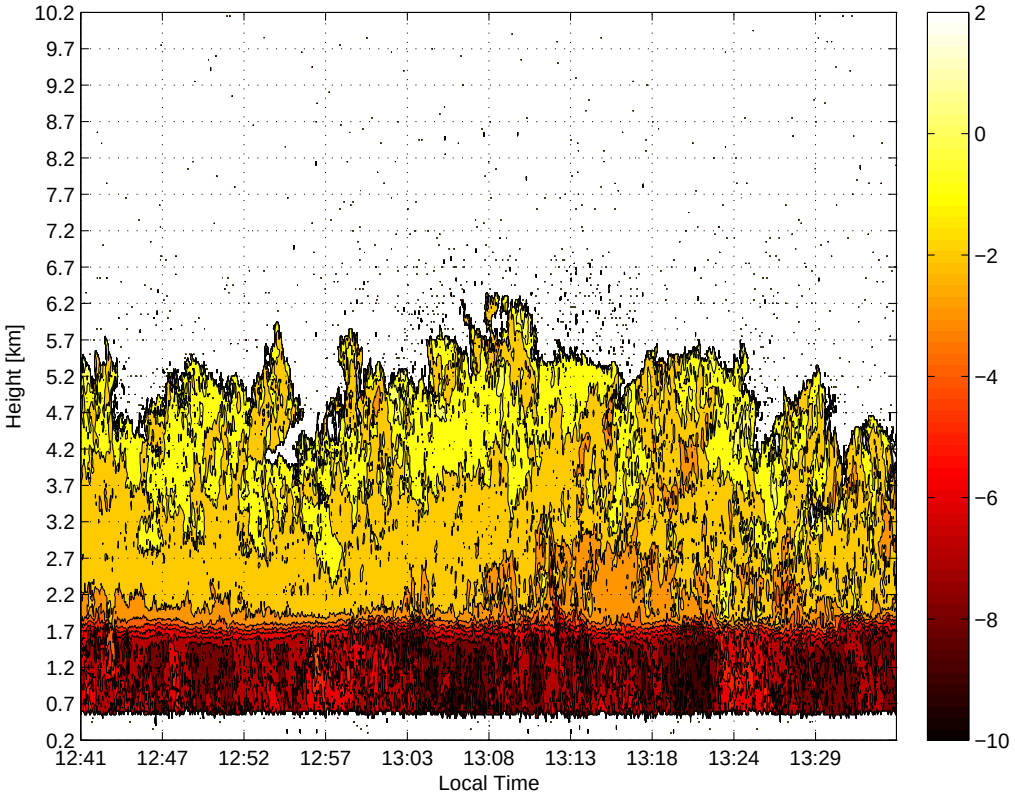

Figure 4.1 *Time - height indicator diagram of Doppler velocity produced by the Järvenpää Doppler radar from 12. September 2007. Light yellow colours indicate small fall speeds (snow), dark red colours indicate higher speeds (rain). Speeds for the lowest altitudes are not measured. This is done to prevent damage to the signal receiver by powerful return signals from scatterers very near to the radar.*

consistent spectrum width values above the freezing level also suggest that there is only a weak relation between the snow flake size and fall speed. The data presented here suggests that snow has a constant fall speed of about $1\frac{m}{s}$ and a spectrum width of about $0.3\frac{m}{s}$. A more precise formula for fall speed would be a linear fit in the form of $V_s(T) = -1.5\frac{m}{s} + \frac{T}{20}\frac{m}{s°C}$. For simplicity, the constant value used in this study.

Rain below the freezing level exhibits very different fall speeds. The speeds vary from around $-3\frac{m}{s}$ to $-7\frac{m}{s}$ and are nearly constant after snowflakes have melted completely. The different fall speed profiles for rain support the assumption that raindrop fall speeds are more sensitive to DSD than those of snowflakes. Spectrum width profiles are also more diverse in rain. For these reasons, a typical fall speed for rain is much more difficult to estimate even for a single rainfall type (here all cases represent stratiform summertime precipitation). When averaged over all cases, the

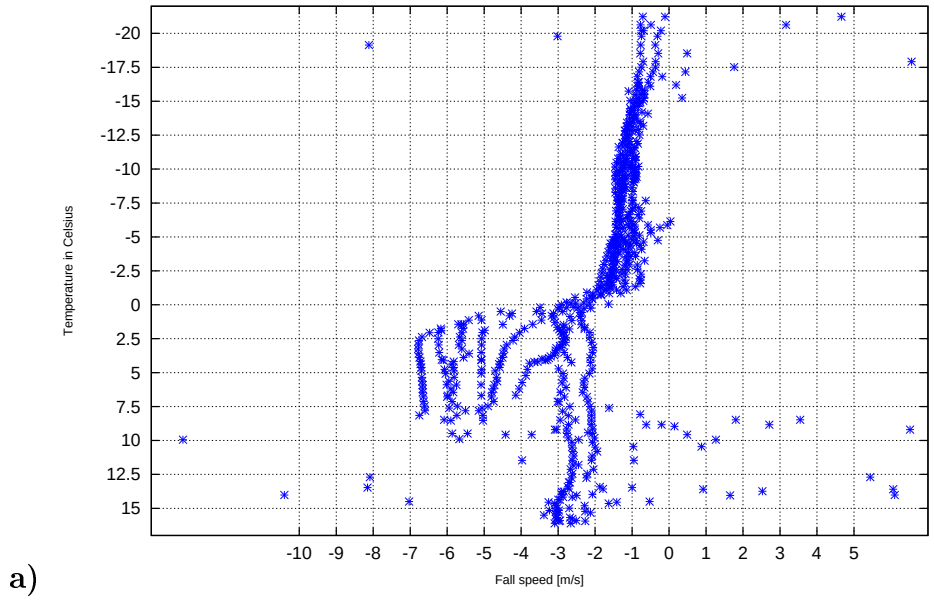

a)

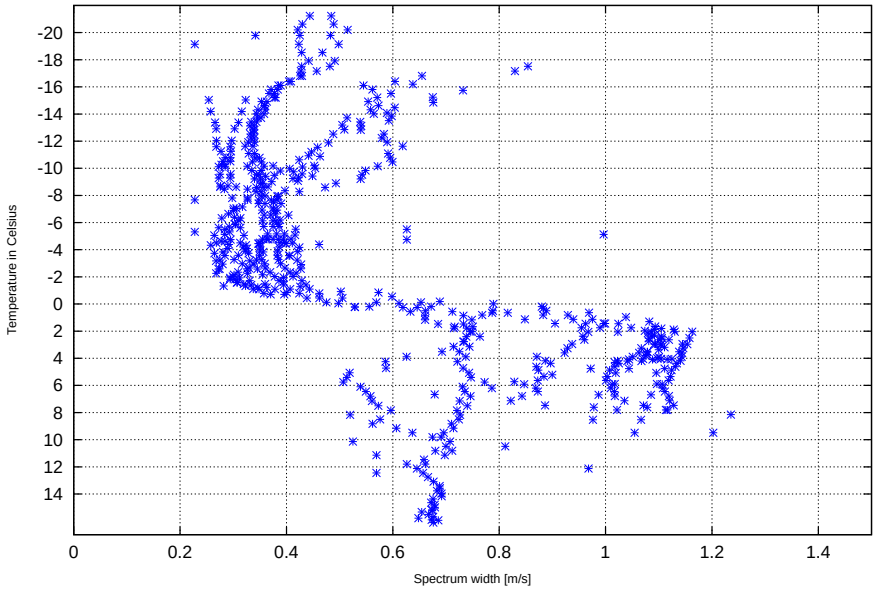

b)

Figure 4.2 **a)** *Measured Doppler fall speed as a function of temperature extracted from the nearest sounding for each case. In snow the profiles are very uniform, whereas in below the freezing level the profiles separate. Different fall speeds in rain are likely the result of differing DSDs.* **b)** *Measured spectrum width as a function of temperature for each case. Spectrum width (and therefore variability in fall speed) is noticeably smaller and uniform in snow than in rain.*

terminal fall speed for rain and the spectrum width are approximately $4.5\frac{m}{s}$ and $1.0\frac{m}{s}$, respectively.

4.2 Sources of wind data

Accurate depiction of the four dimensional wind field is of fundamental importance in reliable calculation of trajectories. There are two principal sources of wind information: direct measurements and numerical weather prediction (NWP) model fields. In this section the pros and cons of different data sources are discussed.

4.2.1 Direct wind measurements

Wind field can be measured in two ways: using radiosonde soundings (*in situ*) or various remote sensing instruments. Soundings are considered the most accurate depiction of the wind field as wind speed and direction can be directly measured from the movements of the sonde. Sondes typically measure wind from few hundred meters to approximately 20 kilometers of altitude every few hundred meters. This allows for a high resolution vertical wind profile from the boundary layer to the stratosphere at the sounding location.

The downside of soundings is the fact that they are rather costly. For this reason the sounding locations are scarce (in Finland, there are three locations) and soundings are performed only every 12 hours. For weather statistics and assimilation for NWP forecasts this interval is appropriate and even mandatory as soundings need to be synchronised with global SYNOP observations. Since wind drift is most important in events of short temporal scale and large spatial resolution, soundings are not sufficient as the only source of wind information.

Doppler radars and wind profilers are the most common remote sensing instruments used to measure the wind field. Both instruments are used in a very similar manner and produce a vertical wind profile at the location of the instrument.

Wind profilers are essentially radars or sodars (Sonic Detection and Ranging) designed to measure vertical wind profiles. Their vertical resolution is comparable to that of soundings, but they can measure wind profiles with a much higher frequency. Their vertical extent and resolution depend on the used frequency. Tropospheric wind profilers generally have operational range of 0.2 - 14 km (US EPA 2000). Sodar-based profilers are generally limited to observe the lower troposphere. Doppler radars

can measure the local wind profile with the VVP method, and can reach altitudes of about 7 - 15 km, provided that scattering ice crystals reach such heights.

4.2.2 NWP model fields

NWP models produce wind fields with varying spatial and temporal resolutions. In this study HIRLAM MB71 (referred to as simply HIRLAM), an operational meso - β scale weather forecasting model at FMI, was utilized (FMI 2008).

The integration area of HIRLAM spans the Northern Europe along with parts of North-Western Russia. The model has grid resolution of 0.068°, and 60 vertical levels spanning from the ground level to approximately 40 kilometers of height. The 0.068°resolution translates to grid box size of roughly 7.5 km x 7.5 km over Finland, with the size decreasing towards the poles. Vertical level spacing increases from about 60 meters near the ground to more than 1 kilometer in the upper troposphere. With the model being used for weather forecasting, the majority of the model levels are below the tropopause. Forecasts are made four times a day at 00 UTC, 06 UTC, 12 UTC and 18 UTC. Each forecast spans 54 hours, with first 12 stored hours at one hour resolution and subsequently with 3 hour resolution. Forecasts from ECMWF (European Centre for Medium-Range Weather Forecasts) Integrated Forecast System are used as boundary conditions. The model is hydrostatic, meaning accelerations in the vertical direction are omitted.

There are several advantages in using model wind fields. The HIRLAM-produced fields are readily available for practically every day of the model's operating time and therefore are a reliable source of wind data. Moreover, the wind data is available with a good and uniform horizontal resolution (the above mentioned 7.5 km) since the model uses a rotated spherical coordinate system where Finland is approximately at the equator. As opposed to radar-based wind measurements, the reliability of model winds is (in the scope of this study) independent of geographical location, and therefore no additional manipulation of the wind field is required.

There are two principal problems with HIRLAM-produced wind data. Firstly, the wind fields are forecasts, and do not necessarily represent the real wind. This problem becomes more severe further from the model initialisation time. Secondly, the maximum temporal resolution of the model data is one hour, limiting the analysis to weather systems of mesoscale and larger.

Both data sources are useful, albeit for different purposes. In this study, soundings are used for climatological studies, whereas model winds are used in case studies,

where accurate spatial representation of the wind field (with satisfactory temporal resolution) is required.

4.3 Trajectory computation method

When the precipitation fall speed, the originating height and the vertical wind profile are known the trajectory of the hydrometeor can be computed. The trajectory tells us the particle wind drift distance relative to the original geographic location as a function of altitude. From the trajectory the displacement (or wind drift distance when the particle has reached the ground), which is generally the quantity of interest, can be determined.

When the vertical wind profile is known, the trajectory can be solved by simply integrating the wind profile in respect to time. In this study this is done separately for the u and v wind components:

$$\Delta X = \sum_{Levels} \Delta x_i = \sum_{Levels} \frac{z_i - z_{i-1}}{w(T)} \left(\frac{u_i + u_{i-1}}{2} \right) \tag{4.1}$$

$$\Delta Y = \sum_{Levels} \Delta y_i = \sum_{Levels} \frac{z_i - z_{i-1}}{w(T)} \left(\frac{v_i + v_{i-1}}{2} \right) \tag{4.2}$$

In the above equation ΔX and ΔY are wind drift displacements in x and y directions, z is height above ground and u and v are the wind components. w is the effective fall speed, which is a function of precipitation phase, and consequently temperature. In the formulas the wind speeds are defined at discrete levels, which is true for soundings and NWP data. The drifts are computed by assuming that the wind speed changes in a linear fashion between successive levels and therefore a simple average between the levels can be used. This method yields satisfactory results if the vertical levels are sufficiently close to one another.

5 Estimation of statistical distribution of wind drift in Finland

To evaluate the magnitude of wind drift in Finnish conditions, a distribution of drift displacements as a function of falling height was compiled. Soundings were chosen as the source of wind data, since they are the best available estimates of the (local) vertical wind profile and are made at regular intervals. Soundings from two locations in Finland (Jokioinen and Sodankylä) were used. Jokioinen is located in South-Western Finland while Sodankylä is located in Lapland. The two locations should therefore cover the whole range of Finnish wind conditions fairly accurately. In order to produce representative statistics, all soundings from years 2007 and 2008 from both locations were obtained. No attempt to identify whether there was actual precipitation during each day was made. Instead, for each sounding we assume a hypothetical hydrometeor that falls from a certain altitude and undergoes phase transitions according to the vertical temperature profile. As precipitation can occur in practically all synoptic weather conditions (perhaps with the exception of winter-time blocking high pressure) the omitting of precipitation detection should not significantly affect the resulting distributions. The sounding data was acquired from FMI's Climate Database.

5.1 The fall speed calculation scheme

As soundings from all seasons are used, all phases of precipitation will be present. Drift distances depend on fall speed (and consequently hydrometeor type) and therefore a model of fall speed behaviour as a function of hydrometeor phase must be developed. In this study, a model based on melting level height and melting layer depth was used. In the model, the melting level height has to fulfil two conditions; Temperature at the level, and the average temperature below the level, must both be greater than zero degrees Celsius. The highest altitude in which both conditions are true is defined as the melting level height. The depth of the melting layer is taken to be 700 meters (coinciding with the typical bright band width presented by Pohjola (2003)). This scheme also estimates the precipitation phase at the ground level, as it depends on the melting level height.

Above and below the melting layer the precipitation is respectively either pure snow or rain, and constant fall speeds presented in section 4.1 were used. In the

melting layer the precipitation is wet snow with varying proportions of water and snow. Within the layer, fall speed is interpolated linearly:

$$W_{sleet}(h) = W_{snow} + \frac{h_Z - h}{D_0}(W_{rain} - W_{snow}) \quad h_Z \geq h \geq (h_Z - D_0)$$

In the above equation h_Z is the height of the melting level and $D_0 = 700$ m.

5.2 Trajectory integration from sounding data

The drift distance integration method used here is based on sounding measurements of geopotential height z, wind speed V, wind direction θ and temperature T. An arbitrary measurement height is chosen and drift displacements are calculated assuming that the hydrometeors fall from this height to the ground (defined as the gpm = 0 isoline). The wind components u and v (zonal and meridional) are calculated from sounding winds and drift distances are accumulated for each component over all sounding levels below the originating height using the Equations 4.1 and 4.2.

The fall speed w is calculated from the temperature profile of the sounding using the method described in section 5.1. To simulate the uncertainty in the fall speed estimate, the displacements were calculated with three fall speeds. namely w_{mean} , $w + \sigma_w$ and $w - \sigma_w$ where σ_w denotes the fall speed spectrum width. If we assume the fall speeds to follow the Gaussian distribution, 68.2% of speeds will fall between the values separated by $2\sigma_w$. Likewise, 68.2% of wind drift displacements will fall between corresponding calculated displacement values. It should be noted that σ_w is different for rain and snow, and for sleet σ_w is interpolated in the same fashion as fall speed (see Eq. 5.1). The possible error in wind estimates is considered to be negligible and to contribute little to the overall error.

The quality of the sounding data can vary greatly, and for this reason a rudimentary data grooming scheme was applied. In order to be included in the analysis, each sounding had to fulfil three conditions:

- The lowest measurement altitude must not exceed 400 meters.
- The sounding must consist of at least 40 measurement altitudes.
- The highest measurement altitude must exceed the predetermined fall height.

These conditions were chosen to ensure a dataset free of obvious measurement errors (such as failed sounding due to defective equipment). After the filtering, a total of approximately 2650 soundings were available for drift displacement computations. The actual number varies slightly with the chosen fall height, as higher altitudes are more "picky" when it comes to the third filter condition.

5.3 Results

The fall height is a factor when calculating wind drift distances. As the identification of true precipitation from the soundings is omitted, the corresponding generating level height is also undefined. Since we are considering the effect of drift to radar measurements, the radar beam height seems a logical choice for the originating level height. This way we can calculate drift distances as a function of the height of a hypothetical radar measurement and consequently range from radar. Distances used range from 10 km to 250 km, the latter being the maximum measuring range of FMI radars. The corresponding fall heights are computed using equation 2.4, with the radar height set to 0 m. The distributions are calculated separately for rain, sleet and snow. The precipitation phase is identified from the vertical temperature profile using equation 5.1.

The radar beam height depends on the antenna elevation angle. Although the elevation angle in PPI scans can be as large as 45°, most scans employ elevations close to the horizon as they provide the greatest effective measuring range. In the analysis, three elevation angles (0.2°, 0.4°, 0.6°) are used.

One of the calculated wind drift distance plots is presented in Fig. 5.1. The lines are cumulative drift probability isolines as a function of distance from radar (or equivalently radar measuring height). The three lines for each isoline represent the distributions calculated from the three fall speeds defined in section 5.2. The complete set of statistics is presented in Appendix A.

Drift distances at fall heights below 500 meters should be taken with a pinch of salt as there are generally very few sounding levels below this altitude and the wind field may not be correctly represented. The nearly constant value of drift distance near the radar is therefore most likely an artifact produced by poor vertical resolution of the soundings at low altitudes. At greater fall heights the median drift increases quasi-exponentially with radar measuring distance.

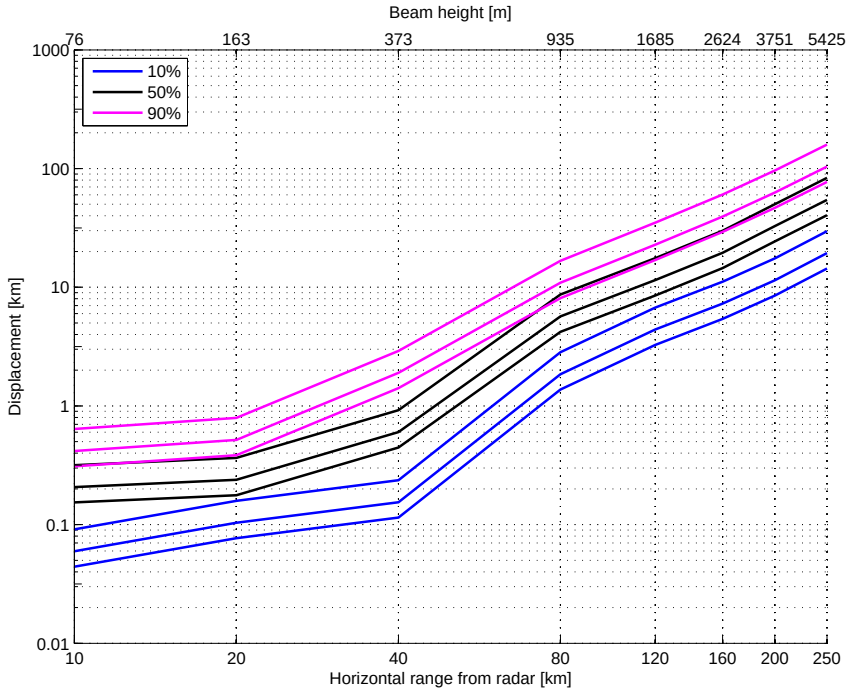

Figure 5.1 *Cumulative probability distribution of wind drift displacements for surface rain and radar beam with 0.4° elevation. The lines represent cumulative probabilities as a function of distance from radar. Each probability is calculated for three fall speeds, w, $w + \sigma_w$ and $w - \sigma_w$ (σ_w denotes the fall speed spectrum width).*

Surprisingly, soundings classified as sleet on the surface produce largest wind drifts. This effect is present in all probability distribution isolines. The fall speed difference can not explain such behaviour, since snow has a lower fall speed and should drift further in a given wind field. This leads us to believe that there is (perhaps unphysical) correlation between large wind speeds and sleet occurrence. Moreover, the probability isolines are generally more closely packed in the case of sleet, indicating that there is less variation in average wind speed from case to case.

When considering stratiform frontal snowfall, the generating level height is generally approximately 4000 meters (Gunn et al. 1954). This translates to a maximum radar measuring distance of approximately 200 km. According to the statistics presented, the expected (median) drift distance from this fall height is in the order of few tens of kilometers. This implies that, when it comes to snow, wind drift becomes significant when measuring precipitation beyond 160 km distance. For applications that need precipitation information with around 1 km resolution this range is even lower.

The uncertainty in hydrometeor fall speeds (represented here by the fall speed spectrum width) introduces error to the wind drift distance calculations. This effect is accounted for by the three isolines for each probability distribution value. The difference in wind drift distances is related to the drop sorting phenomenon discussed in section 3.3. Close to the radar the uncertainty in wind drift distances is roughly a hundred meters, whereas at 160 km range it is approximately 10 kilometers. These differences are very closely similar for all precipitation phases.

6 Trajectory reduction of PPI images to ground level

Trajectories can be used with real events to estimate how well radar PPI images represent the precipitation at ground level. Here a method of producing a ground level radar reflectivity field based on radar PPI images and trajectories computed from the wind field is presented. The reflectivity field produced by trajectory reduction can then be used to estimate the true field at ground level.

There are different ways to reduce reflectivity fields to the ground level. We can either trajectory-reduce a reflectivity field measured at a certain instant to the ground, or we can fix the time stamp for the ground field and integrate the trajectories backwards in time from ground level until they intersect a radar observation aloft. In both cases, the lowest elevation radar PPI is considered the best source of radar data.

The first method was not chosen, as observations further away from the radar take longer time to fall, and therefore the produced ground field does not represent any single observation time, and the reduced ground field is not directly comparable to any PPI image. Also, due to real or computational vertical divergence, the first method may leave some ground pixels unoccupied with data. The second method does not suffer from this, but instead requires a series of radar PPI images from which the ground field is computed. Trajectories from ground locations further away from the radar take significantly more time than the typical radar temporal resolution (5 minutes) to reach the radar measuring volume and for this reason radar measurements from the past (relative to the time stamp) are required.

6.1 Description of the analysis

The radar images used are produced by the FMI Vantaa weather radar. The elevation angle used is 0.3°, and is the lowest operationally available PPI elevation for FMI radars. The radar reflectivity is measured in 500 meter bins with 1.0°angle resolution. With a maximum measuring distance of 250 km, this translates to PPI image resolution of 500 by 360 pixels. The PPI images used in the analysis contain raw reflectivity data and for this reason are not artifact-free, but contain residual clutter, ships and aircraft. An example of radar reflectivity PPI image is presented in Fig. 6.1.

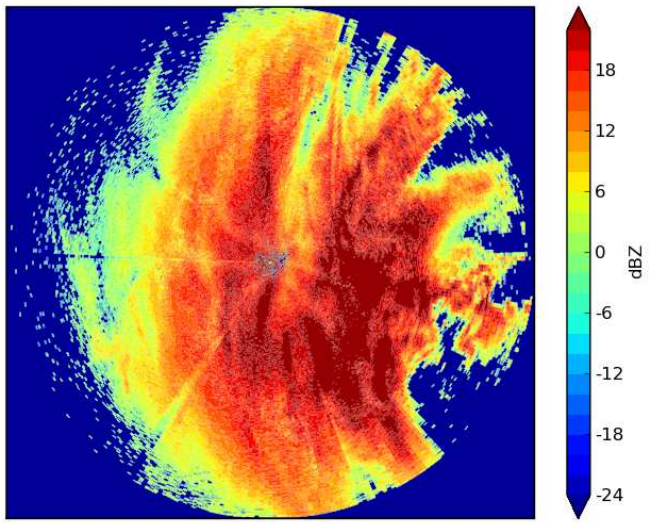

Figure 6.1 *Radar reflectivity PPI of a snowfall case produced by the FMI Vantaa radar. Non-meteorological echoes and partial beam blocking are apparent as distinct clutter near the radar and radial lines of decreased reflectivity. Image was recorded on 23.11.2008.*

The wind field corresponding to each analysed case is extracted from the FMI HIRLAM MB71 model. The extracted winds cover the entire Vantaa radar measuring area using a 60 by 60 grid. In the vertical dimension there are 45 levels spanning from 80 m to about 10 km of altitude. Temporal resolution for the wind field is one hour.

As described previously, the trajectories are computed "from the ground up", meaning the wind field is reversed and the integration is done backwards in time from the ground level. The computation is done using Eq. 4.1 and 4.2, with levels being the model levels. We only analyse cases where the precipitation is pure snow, so the fall speed of snow is used in trajectory computation.

As opposed to sounding data, the model wind field is a true 4-dimensional grid. From this follows that the trajectory at each level is commonly located somewhere between the grid points and we must choose the most representative u and v for each trajectory location in time and space. For time, we use the currently valid field, meaning $V = V(x, y, z, t_i)$ for $t_i \leq t \leq t_{i+1}$. For space, we take the closest grid point (x, y) in the current level z and use the winds $V(x, y, z, t), V(x, y, z+1, t)$

in the integration formulas. The method of choosing the wind field grid points for trajectory computation is illustrated in Fig. 6.2.

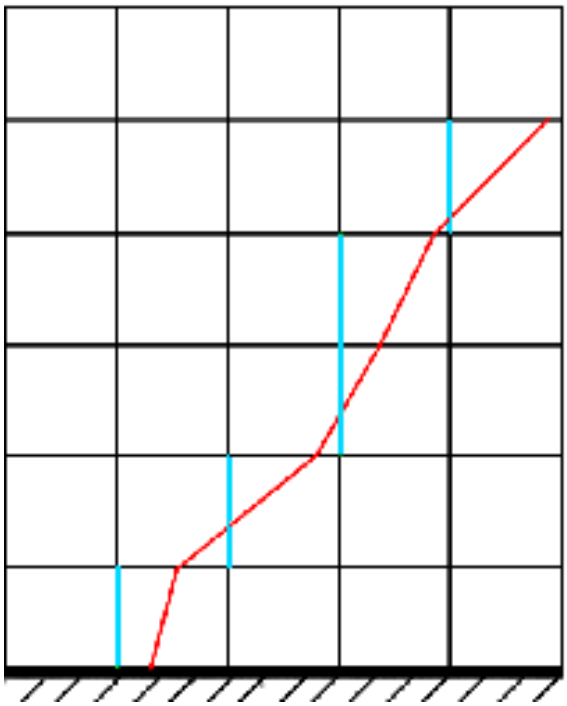

Figure 6.2 *Illustration of the method of choosing the most representative wind speed from gridded wind field. The red line is the computed trajectory and blue lines indicate the wind field grid points used in the computation. Between each level, we use the wind data from grid points* $(x, y, z), (x, y, z + 1)$.

The ground level reflectivity field is constructed by creating a blank 500 by 360 pixel image, and computing a trajectory for each of the pixels according to the wind field. Then the location where each trajectory enters the radar measuring volume (with the volume bottom limit calculated using Eq. 2.4) is determined, in both time and space. The value for each ground field pixel is retrieved from the radar bin nearest to the location where trajectory intersects the radar measuring volume, using a PPI image closest to the intersection time. This way the ground field is calculated pixel wise from the previous PPI images.

There is one significant issue in trajectory reduction which arises from the fact that the method uses data from a single radar. In the upwind side of the radar, the trajectories originating from pixels near maximum radar range tend to intersect the radar volume beyond the radar measuring area. As no reflectivity data is available in these cases, the associated pixels are marked as "unavailable". These unavailable

pixels form an area near the edge of the ground field at the upwind side, with the size and shape of the area depending on the wind field. This effect is not encountered in the downwind side of the radar, as all trajectories originate there from the radar measuring area. The downwind side coverage of the ground level estimate extends beyond the original measurement range. However, this area is "lost" in the present calculation which is performed in the original measurement grid of 500 by 360 bins.

In the calculation it is implicitly assumed that precipitation measured aloft always reaches the ground. Weak precipitation may however evaporate or sublimate before the ground. For this reason small reflectivities at large distances from the radar may not be correctly represented by the ground field, although low reflectivities at large distances can be caused by partial beam filling and therefore may be inaccurate to begin with.

6.2 Results

A trajectory-corrected PPI computed for the snowfall event of 23. November 2008 is presented in Fig. 6.3. The area of unavailable trajectory-corrected data is visible in the northeast in Fig. 6.3 b). Reflectivities near the radar remain nearly unaffected. Further away from the radar the differences are more noticeable, especially in areas directly up-, or downwind from the radar. Features in the measured PPI are somewhat recognizable in the corrected field, although they are heavily distorted with increasing measuring distance. In the downwind side, the corrected reflectivities reach the edge of the radar measuring area producing noticeable differences compared to direct measurements. The differences are most easily visible from a precipitation event with a lot of spatial structure such as the one presented in Fig. 6.4.

The shape and size of the area of unavailable trajectory data can be used to qualitatively describe the prevalent wind field and the magnitude of drift error. The size of the area is proportional to wind speed, whereas its location shows the approximate wind direction and the shape contains information on inhomogeneities in the wind field.

The differences between corrected and measured reflectivity fields are obvious in each individual measurement. However, it is not immediately clear how the cumulative contribution between the two behaves as a function of time. In order to understand the effect of trajectory correction more thoroughly, it is imperative

to study its effect on cumulative snowfall. It was hypothesized in chapter 3.2, that the cumulative difference between corrected and measured snowfall decreases with accumulation time.

As the used trajectory calculation method is unoptimized and therefore computationally intensive, some simplifying assumption about the wind field is needed when studying snow accumulation. As large scale winds generally do not change much in the order of few hours, the trajectory computation scheme can be simplified by assuming a constant wind field in time. Therefore, as a first approximation, the trajectories are also constant when considering accumulation periods of a few hours. From this follows that the trajectories need to be computed only once per accumulation period (taken to be three hours in this study).

The measured reflectivities need to be transformed into snowfall intensities and further again to cumulative snowfall. The $Z_e(S)$ relation used for this purpose is $Z_e = 100S^2$, where S is snowfall in $\frac{\text{mm}}{\text{h}}$. The chosen relation is the one used in FMI radar network when operationally estimating snowfall.

As radar measuring bins (or pixels in radar images) are not of uniform shape or size, the physical bin dimensions must be taken into account when evaluating wind drift. The azimuthal dimension of the bins increases with range because the radar measures in a polar coordinate system. The radial dimension of the bins is constant, however, as the radar beam length does not depend on distance. For this reason

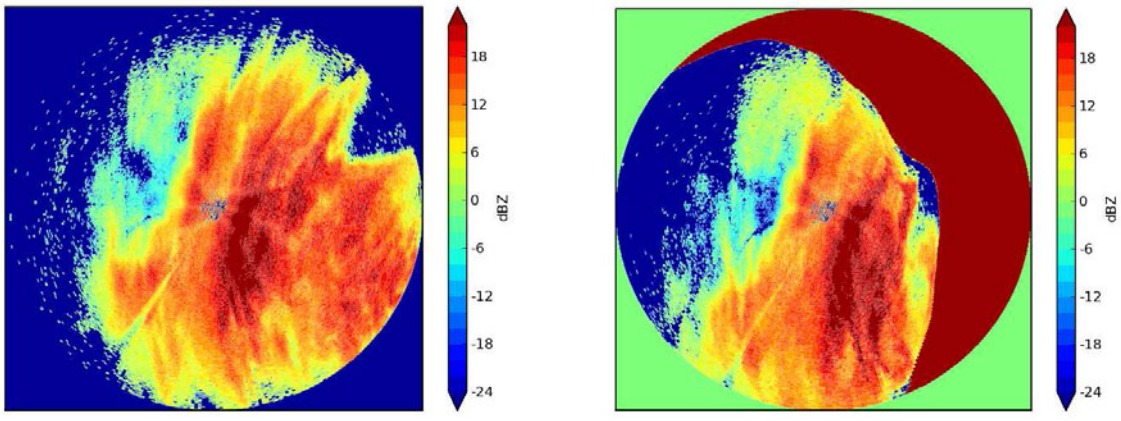

a) **b)**

Figure 6.3 *Two radar PPI images from 23. November 2008, 10:55 UTC. Figure* ***a)*** *indicates radar reflectivity as measured by radar. Figure* ***b)*** *presents the trajectory-corrected ground level estimate for the same time stamp. Dark red colour indicates the area where no trajectory-corrected data is available.*

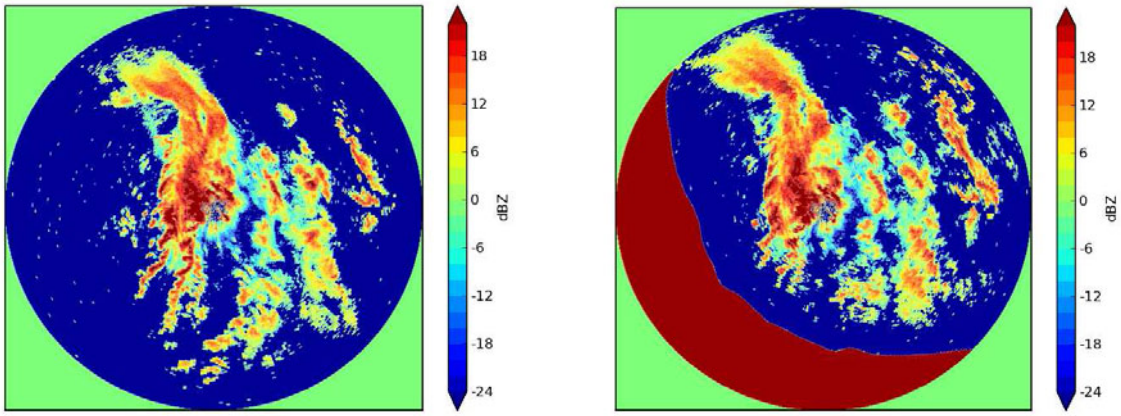

a) b)

Figure 6.4 *Measured and corrected reflectivity field from 2. February 2008, 13:55 UTC. Significant changes in the shape of the precipitating structures can be seen in the trajectory-corrected image. Dark red colour indicates the area where no trajectory-corrected data is available.*

drifts in the radial direction are more easily detected, especially at longer ranges. To eliminate the effect of azimuthal smoothing, the data must be normalized in a way that makes radar bins at different distances meaningfully comparable. In the analysis the physical size of a radar bin at the maximum radar measuring distance (250 km) is used as the reference, and closer to the radar the bins are averaged in azimuthal direction so that bin physical dimensions coincide. It can be easily shown that at 25 km distance one has to average over approximately 10 bins to make the geographical resolution comparable to that at maximum measuring distance.

To evaluate how accumulation length affects differences between directly measured and trajectory-corrected fields the following method was used; Firstly, from the trajectory-corrected field the radar bins where precipitation was detected (exceeding a certain threshold value) were identified and flagged as "available". The resulting field was then divided into subdivisions of constant geographical area, within the accuracy allowed by radar bin dimensions. Finally, all subdivions that have at least 50% data capacity (meaning the number of available radar bins), were compared to the measured field from the same location. The relative amount of subdivisions in the corrected field where there is no precipitation in the corresponding measured field subdivision tells us the importance of trajectory correction. A subdivision where the corrected field detects precipitation but the measured field does not is referred to as "false negative". The relative number of false negatives is a measure

of error between the measured and corrected fields.

The relative amount of false negatives as a function of accumulation time for the 23. November 2008 case is presented in Fig. 6.5. It can be seen that with larger threshold values the relative number of false negatives increases. This can be understood as areas of intense precipitation are generally compact and therefore susceptible to wind drift. Weaker precipitation is usually widespread and the number of false negatives is consequently lower.

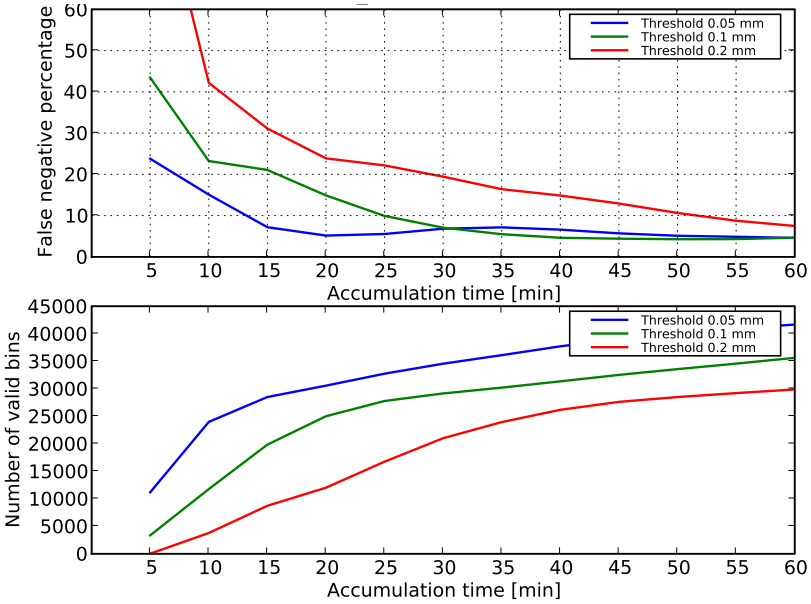

Figure 6.5 *The relative amount of false negatives in the 23. November 2008 case as a function of accumulation time and precipitation threshold value. The subdivisions are normalised to 2 km^2 area. Larger threshold values produce more error, and the error saturates at approximately 10% for all values.*

Furthermore, for all threshold values the error defined as the number of false negatives does not approach zero. This is the result of beam overshooting at large distances from the radar (at the downwind side). In these areas there is constant underestimation of precipitation by the measured field. While at small to medium distances snow accumulation with time reduces the error, at large distances the error remains nearly constant. This saturation value is related to the relative amount of precipitation never directly measured by the radar.

The quality of the analysis was controlled by observing the relative amount of precipitation between measured and corrected fields in the subdivisions deemed as false negatives. It was found that, in the subdivisions deemed as false negatives,

the measured field constantly produced precipitation values less than 50% of the corrected field value.

The 23. November 2008 case represents a truly stratiform snow event. For a case with more small scale spatial structure, the differences can be greater, as can be seen in Fig. 6.6. This supports the claim that convective precipitation events suffer more from wind drift than stratiform events. However, as precipitation events vary greatly in spatial and temporal structure and for this reason the distinction between stratiform and convective precipitation is not always meaningful, the result presented here is qualitative in nature.

The effect of accumulation over time can also be qualitatively seen in Fig. 6.7. The two PPI images present the fraction between corrected and measured precipitation fields after 15 and 180 minutes of accumulation. The short-term accumulation plot shows a lot of detail and sharp differences even at close ranges from the radar. After three hours the field is significantly smoothed, although locations of over- and underestimation remain. This points to the fact that three hours is not sufficient time span for the entire precipitation pattern to pass. One should also note the areas of constant under- and overestimation by the measured field at downwind and

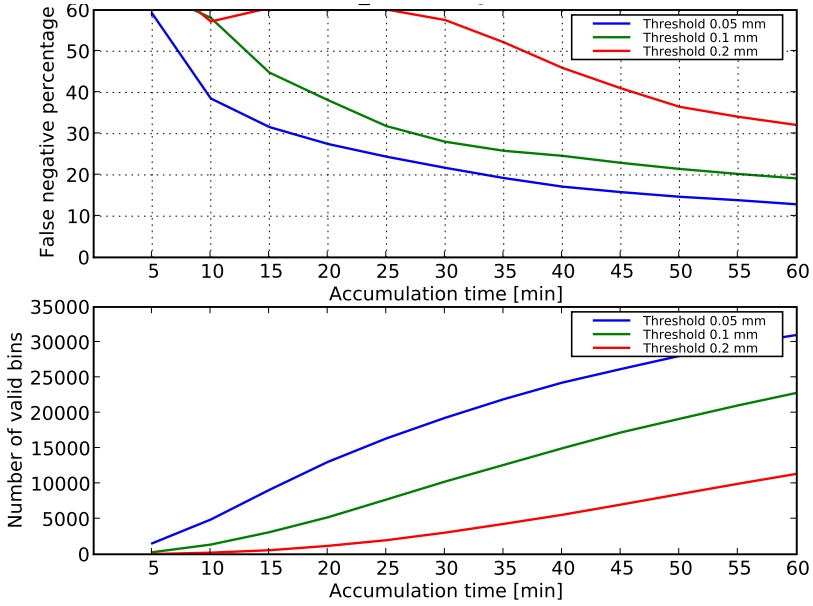

Figure 6.6 *The relative amount of false negatives in the 2. February 2008 case as a function of accumulation time and precipitation threshold value. The subdivisions are normalised to 2 km^2 area. The drift error remains unsaturated for 60 minute accumulation period.*

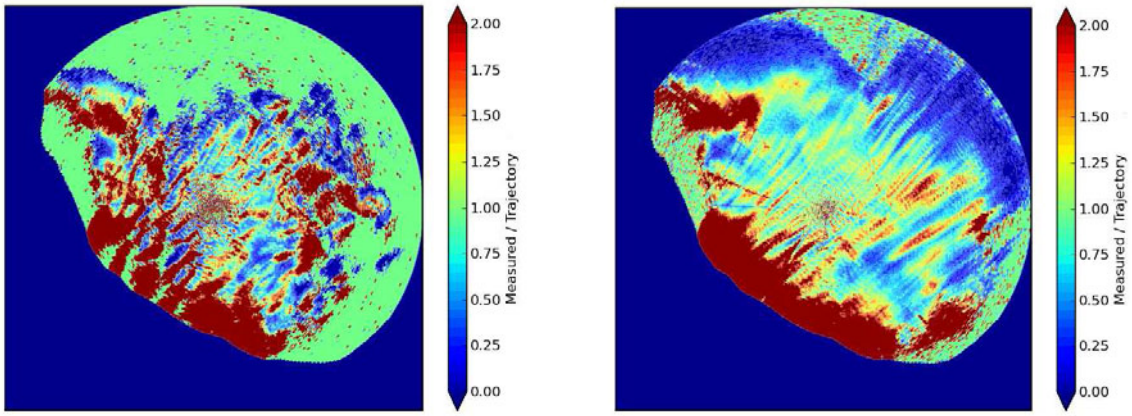

a) b)

Figure 6.7 *Fraction of measured snowfall and trajectory-corrected snowfall for the 2. February 2008 case. Fig a) depicts the difference after 15 minutes of accumulation, while Fig b) depicts the difference after 180 minutes.*

upwind sides of the radar, respectively. These are caused by the beam overshooting at large distances where radar detects very little precipitation from either measured or corrected field.

To further investigate the behaviour of trajectory-correction, Fig. 6.8 illustrates the distribution of the relative difference between corrected and measured snowfall fields as a function of distance from radar for a stratiform case. There is significant scatter at medium distances where the radar beam is sufficiently high for drift to occur, but the beam overshooting does not yet take place. The mean difference is however essentially zero. At large distances the measured field quite constantly produces snowfall amounts less than those produced by the corrected field, as indicated by the long tail towards high values. This effect is amplified with longer accumulation times, which indicates that areas near radar measuring area edge are most susceptible to drift errors. This implies that a quality metric describing the expected wind drifting error in a radar composite, based on the distance to the nearest radar and perhaps wind speed statistics, could be developed.

The structure of the precipitation plays a role in the relative difference between measured and corrected precipitation fields. in Fig. 6.10 the difference distribution for the 2. February 2008 case is presented. The relative differences are larger than in the more stratiform case, especially at longer ranges. This difference can be attributed to the finer structure of the event compared to the 23. November case.

At short to medium distances the measured field produces larger snowfall values

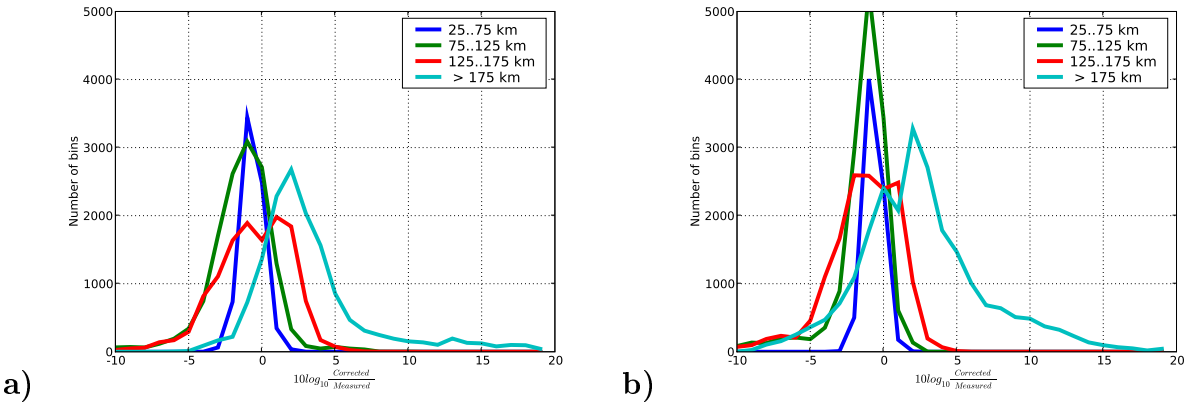

Figure 6.8 *The difference distribution of snowfall after a) 60 minutes and b) 180 minutes of accumulation as a function of measuring distance from 23. November 2008 case. The data bins are normalized to the physical size of a radar bin at 250 km distance. At large distances the trajectory-corrected field is generally more intense.*

than the corrected field, indicated by the small but constant negative bias in the difference field. This is likely to be caused by azimuthal asymmetry in the difference field, which is in turn caused by the radar measuring geometry. At a fixed distance from radar, the trajectories in the upwind side of the radar intersect the radar beam at higher altitudes than those at the downwind side. As reflectivity values generally diminish with altitude, this results in a systematic bias towards higher values (relative to the corrected values) in the measured field at a given range. The effect is illustrated in Fig. 6.9. The effect disappears as soon as the trajectories in the upwind side extend beyond radar measuring range and are no longer included in the analysis.

These above mentioned features are also present in the 2. February 2008 case, although the actual differences as a function of range depend much on the way how the precipitating structures happen to evolve in the accumulation period.

As demonstrated, wind drift has the most profound effect on instant measurements of radar reflectivity. As radar-based visibility products use these instant measurements to estimate local visibility (Dixon et al. 2004), they are likely to benefit from trajectory-correction. Radar-based visibility estimation is done by determining a radar-visibility relationship (or $Z_e(E)$ relationship, where E is the extinction coefficient for visible light) using visibility sensors and radar. Trajectory-correction is likely to improve visibility estimates especially when there are sharp edges in the precipitation field.

To study this, time series of radar reflectivity was calculated for certain locations using both uncorrected and trajectory-corrected data. Based on the shape of the fall streaks (Fig. 3.1), the trajectory-corrected reflectivities should exhibit a phase difference compared to the uncorrected reflectivities, particularly so that the corrected reflectivities lag behind the uncorrected ones. The observed phase difference in minutes represents the error made by assuming purely vertically falling snow.

In Fig. 6.11 time series spanning four hours for a few locations during the precipitation event of 2. February 2008 are presented. The locations were chosen so that top two plots represent locations downwind from the radar, while the bottom two represent locations upwind. All locations are at 75 kilometer distance from the radar, and the two locations at each side are approximately 40 kilometers from one another. A 5 - minute moving average was applied to the time series to reduce noise.

At the upwind side, a phase difference of approximately 5 to 15 minutes is observed. At the downwind side the differences are not easily recognisable. The reason for this is the fact that at the downwind side the trajectories reach the radar mea-

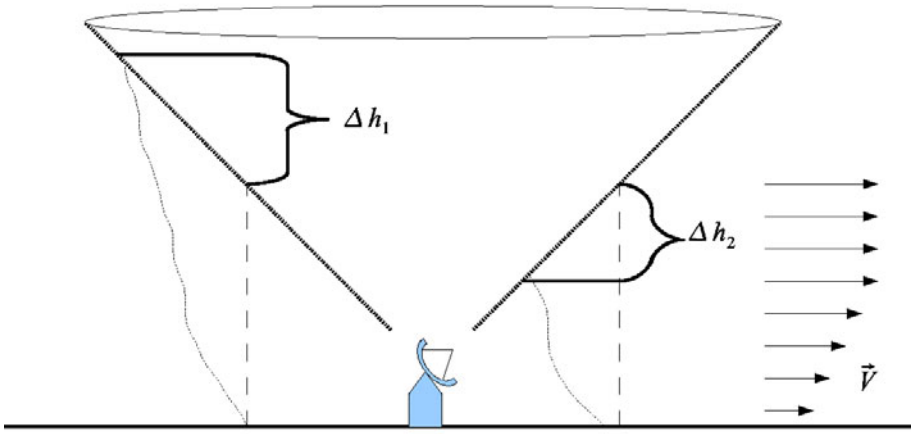

Figure 6.9 *Illustration of the azimuthal asymmetry in trajectory length. When azimuthally averaged, the trajectory-corrected reflectivity values are smaller than the measured ones at a given range (caused by the difference between Δh_1 and Δh_2), assuming a horizontally homogeneous reflectivity field.*

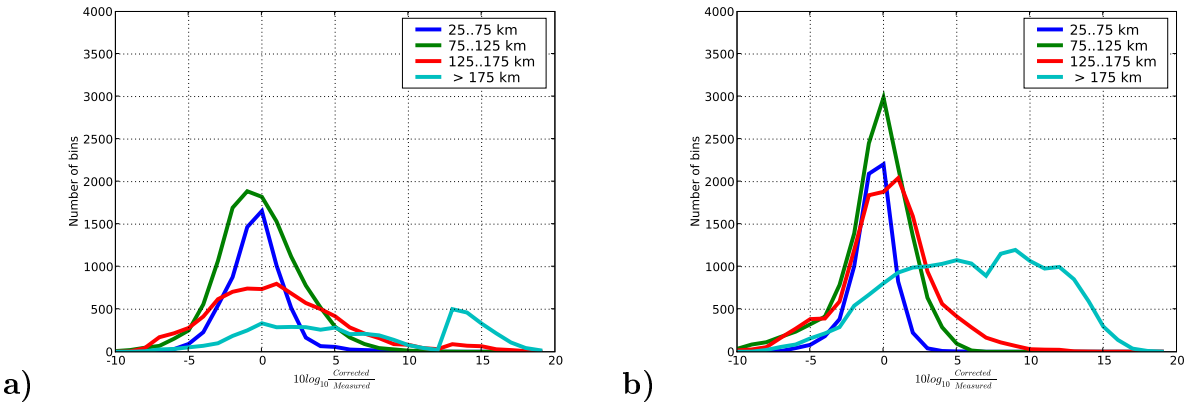

Figure 6.10 *The difference distribution of snowfall after a) 60 minutes and b) 180 minutes of accumulation as a function of measuring distance from 2. February 2008 case. The data bins are normalized to the physical size of a radar bin at 250 km distance. At large distances the trajectory-corrected field is generally more intense.*

suring volume sooner, and drift distances are consequently smaller (see Fig. 6.9). If the distance of the locations from the radar is increased to 125 kilometers, the phase difference becomes apparent also at the downwind side.

The amount of phase difference depends on the structure of the precipitation as well as the measuring range. The stratiform precipitation case of 23. November 2008 produces very small differences in both phase shift and reflectivity, indicating that the scale of the precipitating structures is much larger than the length scale of wind drift. The 30. January 2008 case exhibits the passing of a large scale precipitating system like the one discussed in section 3.2. As the integral $\int Zdt$ is proportional to precipitation amount, the behaviour in the observed case is, at least in qualitative terms, very similar to that of the simple model. The 23. March 2008 exhibits also occasional phase differences. The complete figures are presented in Appendix B.

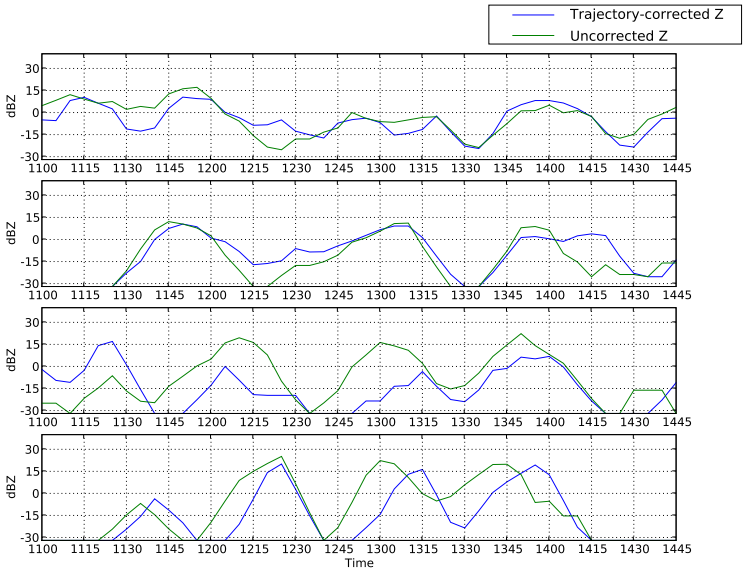

a)

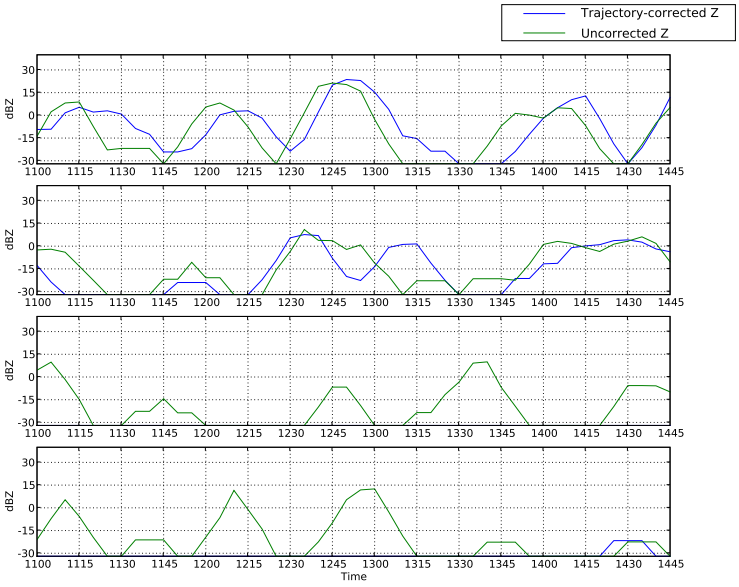

b)

Figure 6.11 *Radar reflectivity time series for four locations calculated from the 2. February 2008 precipitation event. In each figure the top two plots represent locations downwind from the radar, while the bottom two represent the upwind side. Fig a) shows data calculated with 75 kilometer distance from radar, while Fig. b) shows data calculated with 125 kilometer distance.*

7 Contribution of wind drift to the QPE uncertainty

Radar precipitation measurements are operationally corrected using rain gauge networks as the ground truth. This is done to circumvent the problem of unknown DSD which plagues radar based QPE. When radar estimated precipitation is corrected in a way that there is no bias relative to gauge measurements, the accuracy of the radar based precipitation field can be generally improved (e.g. Fulton et al. (1998)).

However, when it comes to rain gauges, the word "ground truth" can be very misleading, especially in the case of snowfall. As described in section 2.4.1, gauges suffer from a variety of error sources which need to be considered in order to make the ground measurements meaningful. Radars have error of their own which cause uncertainties in the measured reflectivities.

To estimate the impact of wind drift correction scheme on the accuracy of a $Z_e(S)$ - relation obtained by a radar - rain gauge pair, a case study was performed. The case of 23. November 2008 was used in the analysis. A low pressure center South-East of Finland produced winds in the order of $10\frac{m}{s}$ and snowfall of around $1\frac{mm}{h}$ (water equivalent). The analysis was performed by estimating the $Z_e(S)$-relation in two ways: from radar data immediately above the gauge and from the trajectory-corrected location. Two stations, Porvoo Harabacka located to the East from Helsinki and Lohja Porla located to the West from Helsinki, were used in conjunction with the FMI Vantaa weather radar. The accumulation times were 12 hours and 10 minutes for Porvoo and 8 hours and 50 minutes for Lohja. Observations were made every 10 minutes. As Harrold et al. (1975) were concerned about the validity of radar point measurements, the obtained Z_e-values are averaged over the 9 pixels around the actual measurement location. Averaging was done in dBZ units in order to diminish the contribution of high Z_e values to the mean value. High solitary Z_e values represent more likely residual clutter than small scale convection in frontal winter episodes such as the one analysed here. The obtained $Z_e(S)$ - relations are presented in Fig.7.1.

In a perfect $Z_e(S)$-relation with zero scatter the data points in log(S)-log(Z) plot form a straight line. For both stations in Fig. 7.1 the trajectory-reduction eliminates some of the scatter, but hardly accounts for all variability. In terms of the correlation coefficient $R(Z_e, S)$, the datasets are improved approximately from 0.47 to 0.53 for Lohja and from 0.46 to 0.56 for Porvoo. It is evident, that while wind drift plays a role in the uncertainty of radar-rain gauge comparison, the other error sources

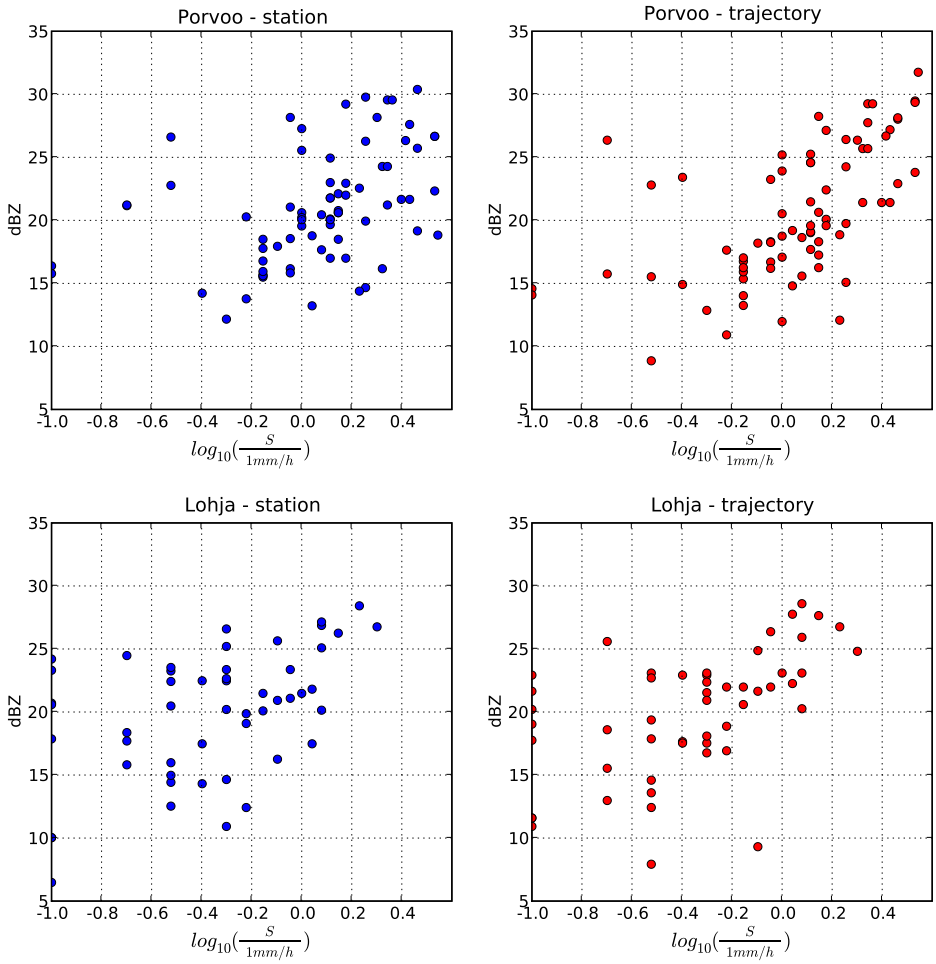

Figure 7.1 *Comparison of equivalent reflectivity Z_e and snowfall rate S pairs from the case of 23. November 2008 for Porvoo and Lohja. Red and blue data points indicate trajectory-corrected and above the gauge Z_e-values, respectively. The accumulation times were approximately 12 and 9 hours respectively for Porvoo and Lohja. The data point scatter is somewhat reduced in the trajectory-corrected plots for both stations.*

and random sampling differences are dominating so that the overall improvement is relatively weak. The case study suggests, that wind drift becomes relatively more important when snowfall intensifies, indicated by the larger improvement for the Porvoo station.

The uncertainties in both radar and gauge measurements translate into errors

in the $Z_e(S)$ relation and consequently in radar based QPE. Therefore it would be useful to understand the impact of wind drift relative to other error sources. The error produced by precipitation wind drift is here introduced as a new error source and its magnitude relative to the other known sources is estimated. The contribution of wind drift error to the variability of the coefficients a and b in $Z_e(S)$ - relationship is of particular interest.

7.1 QPE error sources

There are several uncertainties in measurements done by a radar-rain gauge pair. Gauge errors consist of errors inherent in the measuring equipment and those produced by the behaviour of the precipitation. Uncertainties in radar measurements are produced by calibration errors, attenuation and the *a priori* unknown nature of the precipitation. For further discussion on uncertainties in radar and rain gauge measurements of snow see section 2.4.

The following analysis assumes that the errors in the obtained $Z_e(S)$-relationship are caused by the following individual error sources:

- Error in gauge-measured S.
- Error produced by wind turbulence at the gauge orifice.
- Error in radar-measured Z_e and the subsequently estimated Z.
- Error caused by precipitation wind drift.

Information on errors in gauge and radar measurements is readily available in the literature (e.g. (Austin 1987)). In this analysis the gauge in consideration is the OTT Pluvio weighing rain gauge with a Tretyakov wind shield. Pluvio gauges are a part of the FMI operational rain gauge network. The technical document for the gauge (HACH HYDROMET 2009) states the accuracy of the gauge to be $\pm 1\%$ of the measured value or alternatively ± 0.1mm. The measuring error by radar is typically around 1 dB (see e.g. Bringi and Chandrasekar (2001)). However, it should be noted that such a figure is valid only in ideal conditions. Koistinen et al. (2003) found that sampling differences can introduce gauge-radar discrepancies of 2 - 10 dB in snowfall.

The error by wind turbulence for Tretyakov-shielded gauges was presented in Fig. 2.2. It should be noted, that non-zero wind speed (and therefore turbulence) always

decreases the catch ratio, meaning the gauge will always measure increasingly less snow, relative to the real amount, when wind speed increases. In order to get to the error caused by wind turbulence, the catch ratio distribution at given wind speed must be obtained.

To achieve this, two days worth of high resolution wind measurements from an acoustic anemometer operated by University of Helsinki was used. From the data the typical wind speed variance was computed, using what is known as the structure function or variogram (see section 7.2). This allows us to find the corresponding catch ratio distribution.

Likewise, the contribution of wind drift to the error budget is taken into consideration by using variograms of radar reflectivity over spatial distances. The variograms are used to estimate the spatial variability in the precipitation field, which is related to the uncertainty caused by wind drift.

7.2 The use of variograms to estimate spatial and temporal variability in meteorological fields

The degree of spatial variability in the precipitation field is essential for wind drift to contribute to radar measurement uncertainty. A homogeneous precipitation field produces no effective drift regardless of the wind field. In contrast, very sharp gradients of precipitation intensity make even relatively small drifting distances important to account for. Describing the spatial structure of precipitation, combined with known drift distances, would enable us to draw conclusions about the magnitude of error produced by wind drift.

The variability in meteorological fields such as precipitation is not random, but the fields exhibit *continuity* in both time and space. Measurements spatially or temporally near each other tend to correlate, and this correlation usually decreases with distance. This dependence of correlation (or autocovariance) on distance can be quantified using the structure function (Cressie 1993), also known as the variogram (Germann and Joss 2001). Variogram describes the amount of variance between two simultaneous observations separated by a certain distance, or alternatively between two observations from the same location (using the same sensor) separated by time. This variance is caused solely by the intrinsic variations in the observed field.

The variogram is defined as (Germann and Joss 2001):

$$2\gamma(h) = \text{var}\left\{S(x) - S(x+h)\right\} \tag{7.1}$$

In the formula, $2\gamma(h)$ is the variogram and S the dependent field in question, described as a function of a spatial variable x. Quantity h is the *lag distance* and var{} denotes the variance operator. The lag distance is the separation in space over which the variance in S is calculated. When the Eq. 7.1 is evaluated over several lag distances, the spatial structure of the field is revealed.

The field S can be practically any well defined field, although it should satisfy the condition of *intrinsic stationarity*, meaning that the value of the variogram should only depend on the lag distance h. In other words, the location in which the variogram is calculated should not affect its value. If this is not true, the variogram represents only the region in which it is calculated. This must be kept in mind when drawing conclusions from the information provided by variograms. Furthermore, it is assumed that the Z_e field is isotropic, meaning that the variogram is only a function of distance, and not direction, between two points.

When analysing real two-dimensional fields the definition of the variogram must be modified. In the definition (Eq. 7.1) the lag distance h is a continuous variable, while in real life the we must divide the entire range h into range bins h_k. Now, by replacing h_k with radial separation distance r_k and rewriting the variance operator, we can write the Eq. 7.1 into the form of:

$$2\gamma(r_k) = \frac{1}{N(r_k)} \sum_{i=1}^{N(r_k)} \left[Z_e(x_i) - Z_e(x_i + r)\right]^2 \tag{7.2}$$

Here r_k is the lag distance in question, $N(r_k)$ is the number of observations in the lag distance bin $r_{k-1} \rightarrow r_k$ and Z_e is the equivalent radar reflectivity factor. Essentially, we take all pairs in the reflectivity field that fall into a certain separation range interval and average over their squared differences. This is then done with a variety of range bins r_k to describe the spatial structure of the reflectivity field.

For wind speed, a *temporal* variogram is used. In this case the variogram is computed over time, yielding information about the temporal distribution of wind speeds in a fixed location. This information can be used when estimating wind speed variability over different time scales. As time is a single-dimensional quantity the variogram computation is simple compared to that of radar reflectivity.

The horizontal structure of the Z_e - field depends greatly on the precipitation type. If separate precipitating cells are present, the variogram will increase sharply

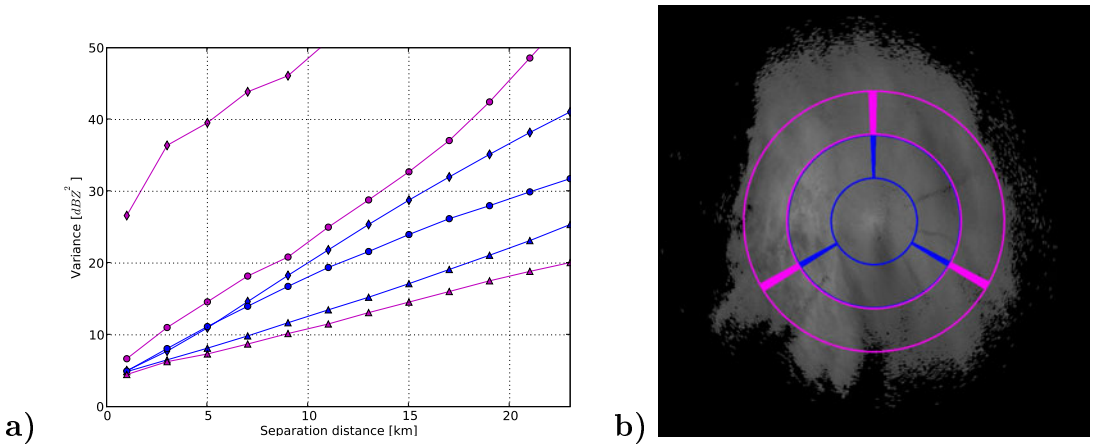

Figure 7.2 *Variograms calculated at different directions and distances from the radar in a stratiform snow case (24. January 2008). The variograms are calculated from 100 by 120 pixel areas indicated by the segments in figure b). In figure a) the colours indicate different range intervals while line symbols indicate different directions;* ▲ *indicates the top right,* ♦ *the middle and* ○ *the top-left direction. The closest 50 kilometers, as well as furthest 100 kilometers, are omitted as clutter near the radar and beam overshooting near the maximum distance produce unrealistic variability in the reflectivity field.*

even at relatively small separation distances, whereas stratiform rain should (somewhat by definition) exhibit smaller spatial variance. One should however keep in mind that the spatial structure of radar reflectivity in PPI images may result from measuring errors such as signal attenuation and beam overshooting.

The variogram is demonstrated in Fig. 7.2 a). In the figure, the variograms are computed for areas of 50 kilometers in radial distance by 120 degrees azimuth. This is done to limit the evaluation time of the analysis, as 2-dimensional variograms are computationally very intensive. The chosen area shape also simplifies the algorithm as radar data is originally in polar coordinates. The area corresponds to approximately 50 km by 160 km geographical area at 77.5 km distance (in the middle of the first range interval). As this is the minimum computation area size (corresponding area increases with distance from radar), the analysis should account for the variability in typical length scales of wind drift displacement (see section 5.3).

The variograms computed from the PPI image in each direction are rather similar and well-behaving at low and medium distances, but at 150 km distance the variograms start to separate. This indicates that the spatial variability of the reflectivity field can be accurately determined only when the radar measures the true precipitation in the entire computation area. At 150 km distance, the edges of the

reflectivity field begin to contribute to the variograms, and the result is no longer representative. The azimuthal dependence in the variograms shows that the reflectivity field is not truly isotropic, even for stratiform precipitation. This can be expected as frontal structures are generally elongated to banded shapes.

7.3 The significance of wind drift to QPE uncertainty

The error contribution analysis was done by simulating radar reflectivity and rain gauge data. The "real" data was generated by assuming a known $Z_e(S)$ relationship and producing 30 data points in the Z_e interval of $[-20, 60]$ dBZ. The 30 measurements represent the amount of radar and gauge data available from a precipitation event lasting approximately three hours. The corresponding S values were then calculated using a $Z_e(S)$ relationship of choice.

This data was then "measured" by applying the known errors to the Z_e and S values generated using the underlying relationship. This was done by estimating the mean and standard deviation for each error source and randomizing the measured Z_e and S around their real values accordingly. The errors were assumed to follow Gaussian distribution. Furthermore, the errors are assumed to be independent from one another, meaning the errors can be independently switched on and off to estimate their relative contribution to the overall uncertainty.

After the 30 measured $Z_e - S$ pairs are generated, a $Z_e(S)$ relationship can be obtained by performing a log-linear least squares fit. In order to obtain statistically significant results, the 30 data point set (and the corresponding $Z_e(S)$ relationship) was generated 1000 times for each analysis. The resulting distributions for the a and b coefficients in the relationship describe the error caused by the measuring errors included in the analysis. The analysis uses an underlying $Z_e(S)$ - relationship in the form of $Z_e = 100S^2$.

The successful implementation of the errors requires that they are described using Gaussian distributions with meaningful mean values and standard deviations. The systematic errors in gauge and radar measurements are described as distributions with zero mean (relative to the true value) and a double standard deviation of $2\sigma = 1.0\%$ and $2\sigma = 1.0$ dBZ for gauge and radar, respectively. The term 2σ is introduced so that approximately 95% of values fall between the presented error boundaries.

The errors by wind drift and turbulence at gauge orifice are in turn represented by Gaussian distributions with standard deviations obtained from variograms. The error means for both quantities are taken to be zero. The variograms for both quantities were computed using data from the same analysed case. Wind speed variograms are computed from measurements with one minute resolution spanning the entire day, while radar reflectivity variograms are computed from a single radar PPI image. The radar image was chosen so that it represents stratiform precipitation as well as possible.

Two cases were analysed in this study, one from 24. January 2008 and another from 30. January 2008. The following example describes the analysis using data from 30. January 2008.

In Fig. 7.3 a time series of wind speed and the associated variogram is presented. The wind speed variability (in terms of variance) at 10 minute separation time, which is the typical temporal resolution of gauge measurements, is approximately $2.6\frac{m^2}{s^2}$.

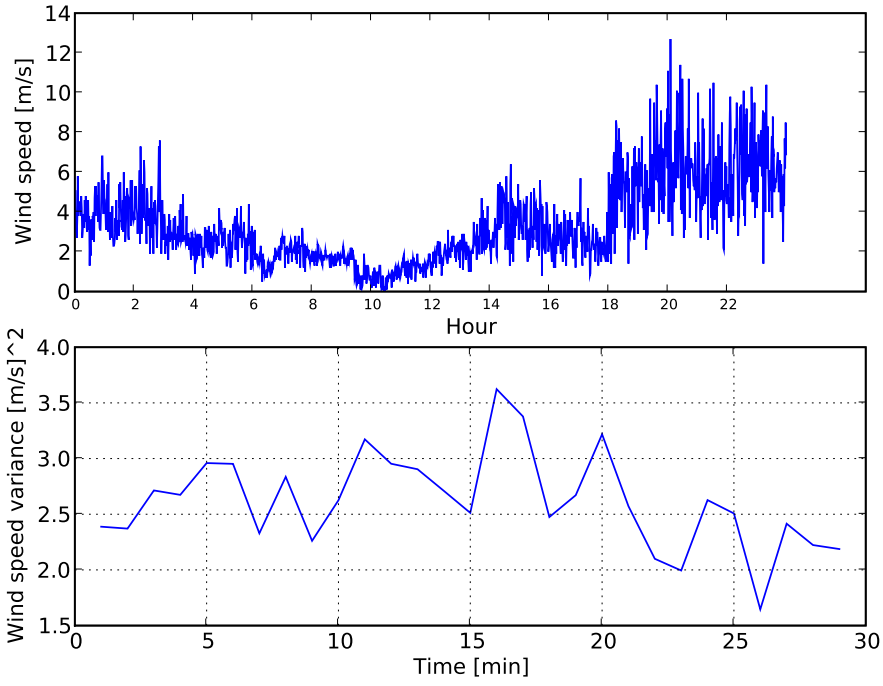

Figure 7.3 *Time series and the associated temporal variogram of wind speed on 30. January 2008. Wind measurements were made at Kumpula campus of the University of Helsinki.*

From the wind speed variance the corresponding standard deviation in gauge catch ratio can be deduced. The formula for catch ratio as a function of wind speed depicted in Fig. 2.2 is (Goodison et al. 1997):

$$CR = 103.11 - 8.67W_s \tag{7.3}$$

Here W_s denotes wind speed. The slight variation of catch ratio with temperature is omitted. From the formula above it immediately follows that:

$$\frac{\partial CR}{\partial W_s} = -8.67 \tag{7.4}$$

$$\Rightarrow \Delta CR = -8.67\Delta W_s \tag{7.5}$$

Eq. 7.5 relates variability in wind speed with variability in the catch ratio by gauge. The standard deviation obtained from the wind speed variogram at 10 minute temporal separation corresponds to CR standard deviation of $\pm 13.9\%$. The mean CR can be calculated from Eq. 7.3, and for $3.0\frac{m}{s}$ wind speed the value is 77.1%.

The wind drift error is characterised by the spatial variance in Z_e combined with drift distance. In Fig. 7.4 a set of variograms computed from radar image depicting the precipitation event is presented. The variances, as depicted by variograms, depend on measuring distance as well as direction. The variograms at the bottom of the figure are rather closely grouped, indicating less uncertainties by non-isotropic precipitation field and measurement errors. These variograms were therefore deemed most reliable for further analysis.

The wind drift error depends on the distance between the radar and the gauge, as larger distance translates to higher radar beam and more wind drift. For this reason drift distances at varying radar ranges were calculated using sounding wind data from the day in question. The corresponding standard deviations in Z_e due to wind drift were then subjectively estimated from the variograms of Z_e with drift distances corresponding to the separation distances in the variogram. This produces an estimation of wind drift error as a function of radar measuring distance. The wind drift at near-zero drift distances was obtained by subjectively extrapolating the variograms to zero drift distance. This was done since soundings do not have sufficient vertical resolution to reproduce the wind field (and the corresponding drift distance) at heights below approximately 500 meters.

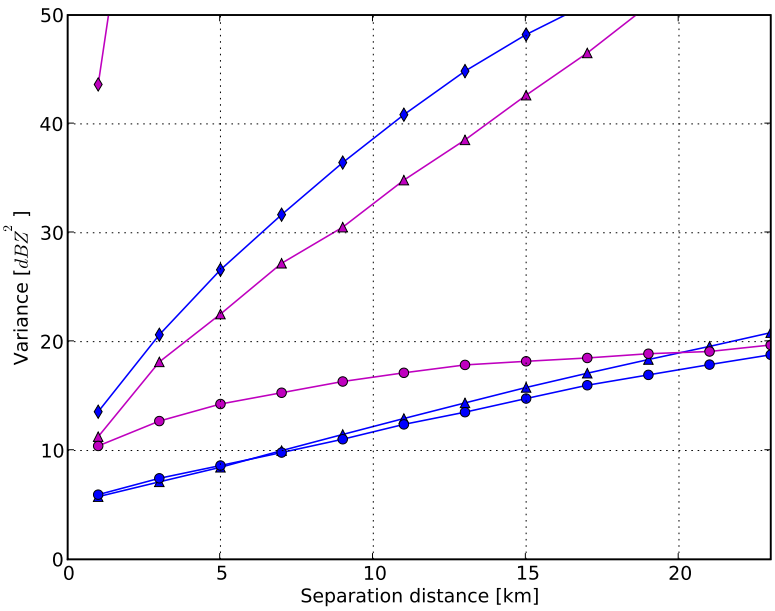

Figure 7.4 *Variogram of radar reflectivity Z on 30. January 2008. The radar image from which the variograms were computed was recorded at 14:20 UTC. Line colors denote average measuring distance: blue line denotes 75 km, magenta line 125 km. Different line markers indicate measuring direction.*

The values each error source for the analysed case are gathered in Table 7.1. These errors were applied to simulated Z and S values to estimate the effect of imperfect measurements to the obtained $Z_e(S)$ - relationship. All errors are proportional to the real snowfall rate, although this is not explicitly indicated in the Z_e-related errors in Table 7.1, as these errors are expressed in logarithmic units and are therefore simply added to the underlying Z_e value. The wind drift error is a function of range from radar, and is presented for measuring range of 75 km.

Gauge systematic error:	$G(S_0, 0.005S_0)$[mm]
Gauge turbulence error:	$G(0.771S_0, 0.139S_0)$[mm]
Radar systematic error:	$G(0, 1.0)$ [dBZ]
Wind drift error:	$G(0, 3.0)$ [dBZ]

Table 7.1 *Values for error sources in the 30. January 2008 case. $G(\mu, \sigma)$ denotes Gaussian distribution with mean μ and standard deviation of σ. S_0 indicates the true snowfall value.*

Error contribution was determined by computing one thousand simulated $Z_e(S)$ - relationships for each error source separately, after which the bias and standard deviation in the distributions of coefficients a and b (constant and log-linear, respectively) were calculated. The deviations represent the error in the $Z_e(S)$ relation produced by each error source. Relative contribution is given by comparing the deviation to the combined deviation by all four error sources. This process was repeated for several ranges from radar.

One set of distributions for a and b coefficients for each error source is presented in Fig. 7.5, using error magnitudes from Table 7.1. For both coefficients the dominating effects are turbulence at gauge orifice and wind drift. For the log-linear coefficient b, wind drift error produces the largest deviation from the true value, whereas in the constant coefficient a both effects are equally matched. The deviation in the distribution of a produced by gauge turbulence is approximately half of that by wind drift. It should be noted that gauge turbulence produces significant bias in the distribution of a, as it causes the gauge to constantly underestimate the snowfall.

The relative importance of each error source for the 30. January 2008 case as a function of range from radar is depicted in Fig. 7.7 a). The figure shows the standard deviation of each error source relative to that of all errors combined. The combined standard deviation is calculated using

$$S_{tot} = \sqrt{\sum_i S_i^2}$$

where S_{tot} denotes the combined standard deviation and S_i denotes standard deviations of the individual error sources. It should be noted that the relative contributions do not add to unity because of the nonlinear nature of the combined standard deviation.

In the analysed case gauge turbulence error dominates in the a coefficient at short ranges and produces no less than half of the combined deviation at any range. The wind drift error starts to dominate at ranges greater than 75 kilometers.

In the coefficient b, wind drift dominates other errors at all distances. At close range gauge turbulence and wind drift are more or less evenly matched, but at 100 kilometer distance and beyond wind drift produces deviation of nearly three times that of gauge turbulence. For both coefficients, systematic errors in gauge and radar play a minor part, with systematic gauge error being barely noticeable. One should however keep in mind the assumptions made about the magnitudes of both errors.

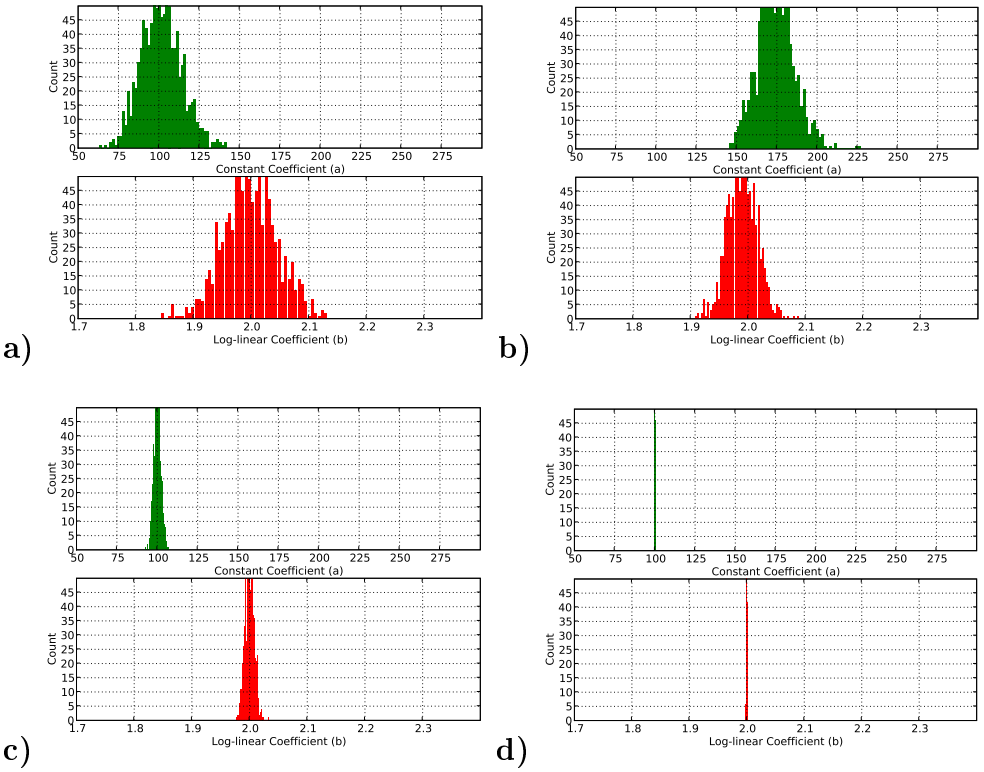

Figure 7.5 *Distributions for $Z_e(S)$ - relationship coefficients caused by independent error sources. Error sources depicted are: a) Wind drift error, b) Gauge turbulence error, c) Radar measuring error and d) Gauge measuring error. Distributions are computed from a data set of 1000 simulated $Z_e(S)$ - relationships. The true data is generated using the relation $Z_e = 100S^2$. Analysed case occurred 30. January 2008 and drift error was calculated at 75 kilometer distance.*

To understand how an increase in wind speed affects the relative error magnitudes the analysis was repeated for another snowfall case. The chosen case is 24. January 2008. The measured wind speeds and calculated radar reflectivity variograms are presented in Fig. 7.6. The main difference compared to the 30. January case is the wind speed, which is on average nearly twice as high at ground level. It can be seen from Fig. 7.6 a) that also the variability in wind speed is twice as high than in 30. January case.

The resulting values for each error source for the 24. January case is presented in Table 7.2. Again, the wind drift error is presented for 75 kilometer range.

Both gauge turbulence error and wind drift error increase in magnitude as the average wind speed increases. However, the wind speed in this case is sufficiently high to reduce the catch ratio by more than 100%. This indicates that the we have

Gauge systematic error:	$G(S_0, 0.005S_0)$[mm]
Gauge turbulence error:	$G(0.571S_0, 0.237S_0)$[mm]
Radar systematic error:	$G(0, 1.0)$ [dBZ]
Wind drift error:	$G(0, 3.87)$ [dBZ]

Table 7.2 *Values for error sources in the 24. January 2008 case. $G(\mu, \sigma)$ denotes Gaussian distribution with mean μ and standard deviation of σ. S_0 indicates the true snowfall value.*

exceeded the domain of applicability of the gauge turbulence error parametrisation (Eq. 7.3). For this reason only Z-S pairs with positive S values were considered. The resulting standard deviations for each error as a function of radar range are presented in Fig. 7.7 b).

The error contributions of 24. January case are drastically different from those of 30. January case. In the coefficient a, the gauge turbulence dominates at all distances, with wind drift producing about half of the deviation produced by gauge turbulence at the most. For the coefficient b, gauge turbulence dominates near the radar, but wind drift catches up at 75 kilometer range and dominates from there.

The error contribution analysis seems to indicate that error caused by wind drift is on a par with the error by wind turbulence at gauge orifice at all distances. As the latter is acknowledged as a significant issue in gauge measurements of snow, it is implied that wind drift is an equally serious problem.

The two analysed cases indicate that the magnitude of wind speed is of great importance when estimating the relative contributions of the error sources. The two coefficients behave differently, however. The log-linear coefficient b is more susceptible to errors in radar reflectivity, as indicated by larger contributions by radar measuring error and wind drift error. Unsurprisingly, wind drift becomes more important with increasing range from radar, but more so for the coefficient b. The wind drift error seems to contribute the most with relatively low wind speeds in the order of 2–3 $\frac{m}{s}$. At 5 $\frac{m}{s}$ the gauge turbulence error dominates, resulting from the increase in both average wind speed as well as its variability. This indicates that gauge turbulence error increases faster than wind drift with average wind speed. Wind speed greater than 5 $\frac{m}{s}$ at ground level will most likely make any attempts to estimate $Z_e(S)$ - relationships using a radar-gauge pair futile, because of the error (both deviation and bias) produced by gauge turbulence.

The error contribution analysis presented here only accounts for the standard

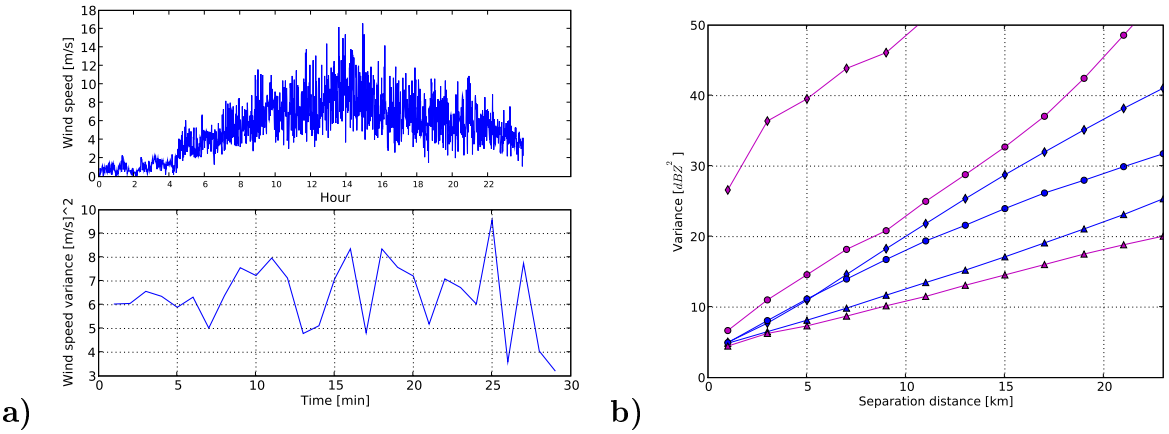

Figure 7.6 *Variograms for wind speed and radar reflectivity factor for the 24. January 2008 case.*

deviation in the distributions of coefficients a and b. The only significant bias in the distributions is in the coefficient a and is caused solely by gauge turbulence. This bias increases significantly with increasing wind speed, as demonstrated by Eq. 7.3. The bias causes underestimation of the snowfall by the gauge.

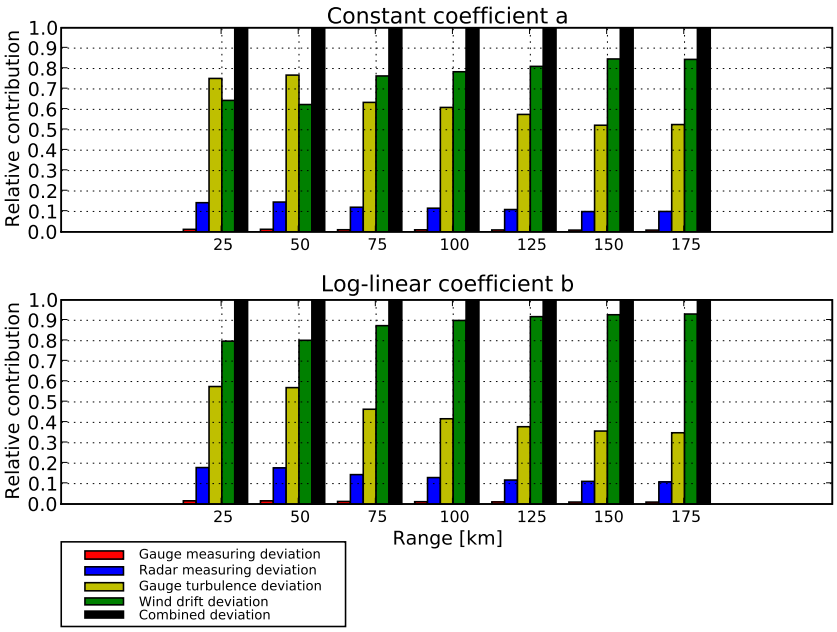

a)

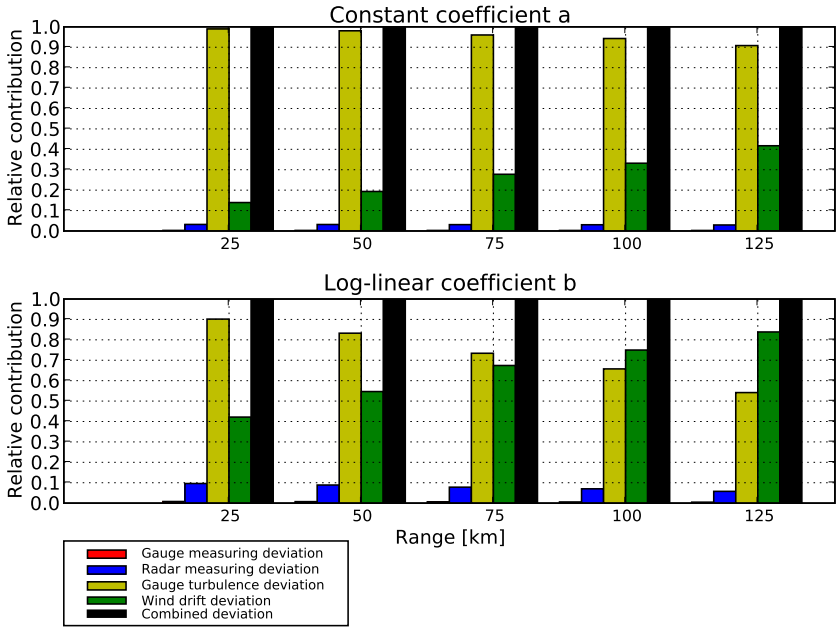

b)

Figure 7.7 *Standard deviations of different error sources relative to that of all errors combined for $Z_e(S)$ - relationship coefficients a and b as a function of range from radar. Fig a) presents results for case of 30. January 2008, Fig. b) for case of 24. January 2008.*

8 Discussion and concluding remarks

Based on the data presented in this study, the effect of wind drift on radar measurements of precipitation varies from negligible to significant depending on a variety of factors. These factors include, yet are not limited to, the spatial structure of precipitation, the prevailing wind field, precipitation phase, radar measuring distance, and the desired spatial and temporal accuracy of the end product. The effect is therefore strongly case- and application sensitive, and it is unlikely that any kind of general measure of wind drift error can be found. However, some general observations about wind drift can be made based on the findings of this study.

The median wind drift distance in Finland exceeds 1 kilometer mark at a radar measuring distance of around 60 kilometers, while 10 kilometer mark is exceeded at around 100 kilometer distance. These two measuring ranges represent the ones where wind drift should be taken into account for high- and medium resolution hydrological products, respectively. Drift distances increase quasi-exponentially with the measuring range, and at the maximum distance of 250 kilometers the mean drift distance is in the order of tens of kilometers for all hydrometeor phases. The windiest 10% of the analysed soundings exhibit drift distances exceeding 100 kilometers at 250 kilometer measuring range. Mittermaier et al. (2004) observed snowfall drift displacements 10-20 kilometers with an average fall distance of 2.8 kilometers. These results agree with the drift displacement statistics presented in this study.

When trajectory-correction is applied, its effects are obvious when considering instant measurements of radar reflectivity and instant quantities derived from it, mainly precipitation intensity and visibility in snowfall. When a single radar is used, an area of unavailable bins appears at the upwind side of the radar. This area is caused by trajectories exiting the radar measuring area before intersecting with the lowest PPI. The shape, size and location of the area depends on the wind field. On the other hand, areas at the downwind side of the radar see improvements in the representativeness of the reflectivity field, as the precipitation originates from areas closer to the radar. Both effects become increasingly apparent with distance from radar. At the downwind side, areas near the edge of the radar measuring area receive the largest benefits.

Lack and Fox (2007) presented cumulative differences between raw rainfall data from CAPPI measurements and drift-corrected rainfall. While they considered a much smaller measuring area and pure rainfall, the cumulative differences in their

study behave in a qualitatively similar way with the precipitation patterns in Fig. 6.7.

PPI trajectory-correction reveals one shortcoming in using a single radar for snowfall detection. When moderate winds are present, as much as 20% of the radar measuring area can receive surface snowfall that is undetectable by the radar. On the other hand, the measuring range in the downwind side is actually longer than the technical limit. When the radar measuring area is fixed, the net effect is a reduction in effective radar measuring area. However, in many cases the nominal outer range of radar measurements could be expanded downwind by applying wind drift correction.

The effect of wind drift on radar-measured QPE was defined by its contribution to the standard deviation of distributions of coefficient a and b in the $Z_e(S)$ - relationship. This effect as well depends on the structure of the precipitation and radar measuring distance. Additionally, wind drift seems to have a more profound effect on the log-linear coefficient b. Near the radar, wind drift is nearly on par with wind turbulence at the gauge orifice as an error source, although with wind speeds exceeding $5\frac{m}{s}$ the gauge turbulence is the dominating error. Turbulence at the gauge orifice produces a notable underestimation bias in snow measurements.

The trajectory calculation method introduced in this work, if properly optimized, could be used to operationally correct single radar PPI images using the currently valid wind field from a weather forecasting model. It is however questionable whether the method can be expanded to cover an entire radar network. A multi-radar trajectory correction using model winds may become unpractically intensive to compute operationally. However, trajectory-correction could be computed for certain locations of interest (e.g. airports or highways) where real-time determination of visibility or snowfall rate is crucial.

This study supports the hypothesis that fine resolution radar measurements of a precipitating system with much small scale structure are most prone to uncertainties by wind drift. This in turn supports the claim that products such as visibility and nowcasting of convective precipitation would benefit the most from wind drift correction.

The correction method used in this study is purely diagnostic, meaning it can not be used to forecast where the precipitation measured aloft falls. Such a product could be implemented using a method along the lines of Rasmussen et al. (2003). In this method the wind field would be estimated from radar CAPPI images and the

measured echoes are advected with the wind. Ground based wind measurements (where available) could be used to assist in wind field estimation. Using the estimated wind field and an assumed vertical wind profile the trajectories could be calculated and the ground precipitation field constructed. In this case the ground field should be calculated using the fall streaks (i.e. from echo to ground using winds $V - V_{sr}$ in Fig. 3.4) to produce the current ground field. This kind of method, albeit less accurate than one using "real" trajectories, should be fast enough to be produced operationally over an entire radar network, even in a grid with 1 km^2 resolution.

In order to understand the effect of wind drift more thoroughly, *in situ* instruments should be used in conjunction with radar to validate the mostly radar-based findings of this study. Especially precipitation and visibility measurements with high (in the order of few minutes) temporal resolution would be useful. Additionally, the trajectory-correction should be implemented in a network of radars. The use of multiple radars would enable the study of wind drift over a much larger geographical area, possibly yielding further insight on the effect of wind drift on precipitation and visibility products in an operational radar network.

The implementation of drift correction to operational products will face additional challenges. In this study drift-correction was applied to pure snowfall cases. The next step would be to take precipitation phase transitions into account. This would involve identifying the melting layer either from radar measurements or model data and correcting the hydrometeor fall velocity accordingly. This adds extra complexity to the algorithm and may or may not be feasible. The fall speeds themselves depend on the precipitation type and phase and may produce notable uncertainties in drift distances. Based on the fall speed data from section 4.1, variability in fall speeds is greatest in the liquid phase, and rainfall is therefore most prone to uncertainties. Correct identification of atypical precipitation such as virga and hail, as well as VPR correction (preferably along the fall streaks, see Mittermaier et al. (2004)) are also important, as they are currently unaccounted for.

Bibliography

Atlas, D., R. C. Srivastava and R. S. Sekhon, 1973: Doppler Radar Characteristics of Precipitation at Vertical Incidence. *Reviews of Geophysics and Space Physics*, **11**, 1–+.

Austin, P. M., 1987: Relation between Measured Radar Reflectivity and Surface Rainfall. *Monthly Weather Review*, **115**, 1053–+.

Battan, L., 1973: *Radar observation of the atmosphere*. University of Chicago press Chicago.

Bringi, V. N. and V. Chandrasekar, 2001: *Polarimetric Doppler Weather Radar*.

Collier, C. G., 1999: The impact of wind drift on the utility of very high spatial resolution radar data over urban areas. *Physics and Chemistry of the Earth B*, **24**, 889–893.

Cressie, N., 1993: Statistics for Spatial data, 900 pp.

Dixon, M., R. Rasmussen and S. Landolt, 2004: Short-term forecasting of airport surface visibility using radar and ASOS. In: *11th conference on aviation, range, and aerospace, Hyannis, MA*, pp. 4–7.

Fabry, F., 1993: Wind-Profile Estimation by Conventional Radars. *Journal of Applied Meteorology*, **32**, 40–49.

Fabry, F., A. Bellon, M. Duncan and G. Austin, 1994: High resolution rainfall measurements by radar for very small basins: the sampling problem reexamined. *Journal of Hydrology(Amsterdam)*, **161**(1), 415–428.

FMI, 2008: *Joint WMO Technical Progress Report on the Global Data Processing and Forecasting System and Numerical Weather Prediction Research Activities for 2008*. Finnish Meteorological Institute.

Fulton, R. A., J. P. Breidenbach, D. Seo, D. A. Miller and T. O'Bannon, 1998: The WSR-88D Rainfall Algorithm. *Weather and Forecasting*, **13**, 377–395.

Germann, U. and J. Joss, 2001: Variograms of Radar Reflectivity to Describe the Spatial Continuity of Alpine Precipitation. *Journal of Applied Meteorology*, **40**, 1042–1059.

Goodison, B., P. Louie and D. Yang, 1997: The WMO Solid Precipitation Measurement Intercomparison. *World Meteorological Organization - PUBLICATIONS-WMO TD*, pp. 65–70.

Gunn, K. L. S., M. P. Langleben, A. S. Dennis and B. A. Power, 1954: Radar Evidence of a Generating Level for Snow. *Journal of Atmospheric Sciences*, **11**, 20–26.

Gunn, R. E. S. and J. S. Marshall, 1955: The Effect of Wind Shear on Falling Precipitation. *Journal of Atmospheric Sciences*, **12**, 339–349.

HACH HYDROMET, 2009: OTT Pluvio technical specifications. `http://www.hydrolab.com/specs/precipitationgauge.asp`.

Harrold, T., C. Nicholas and C. Collier, 1975: The measurement of heavy rainfall over small catchments using radar. *Hydrological Sciences Bulletin*, **20**, 69–76.

Koistinen, J., H. Pohjola and H. Hohti, 2003: Vertical reflectivity profile classification and correction in radar composites in Finland. In: *31st Conference on Radar Meteorology, Seattle*, pp. 534–537.

Lack, S. A. and N. I. Fox, 2007: An examination of the effect of wind-drift on radar-derived surface rainfall estimations. *Atmospheric Research*, **85**, 217–229.

Löffler-Mang, M. and J. Joss, 2000: An Optical Disdrometer for Measuring Size and Velocity of Hydrometeors. *Journal of Atmospheric and Oceanic Technology*, **17**, 130–+.

Marshall, J. S., 1953: Precipitation Trajectories and Patterns. *Journal of Atmospheric Sciences*, **10**, 25–29.

Mittermaier, P. M., J. R. Hogan and J. A. Illingworth, 2004: Using mesoscale model winds for correcting wind-drift errors in radar estimates of surface rainfall. *Quarterly Journal of the Royal Meteorological Society*, **130**, 2105–2123.

Pohjola, H., 2003: *Tutkaheijastuvuustekijän pystyjakauma Suomessa ja sen vaikutus tutkan sademittauksen tarkkuuteen.* Master's thesis, University of Helsinki.

Rasmussen, R., M. Dixon, S. Vasiloff, F. Hage, S. Knight, J. Vivekanandan and M. Xu, 2003: Snow Nowcasting Using a Real-Time Correlation of Radar Re-

flectivity with Snow Gauge Accumulation. *Journal of Applied Meteorology*, **42**, 20–36.

Sekhon, R. S. and R. C. Srivastava, 1971: Doppler Radar Observations of Drop-Size Distributions in a Thunderstorm. *Journal of Atmospheric Sciences*, **28**, 983–994.

Smith, P. L., 1984: Equivalent Radar Reflectivity Factors for Snow and Ice Particles. *Journal of Applied Meteorology*, **23**, 1258–1260.

US EPA, 2000: *Meteorological monitoring guidance for regulatory modeling applications*. US Environmental Protection Agency, Office of Air Quality Planning and Standards Research Triangle Park, NC.

Waldteufel, P. and H. Corbin, 1979: On the Analysis of Single-Doppler Radar Data. *Journal of Applied Meteorology*, **18**, 532–542.

Appendix A

Calculated wind drift displacement statistics from years 2007 and 2008

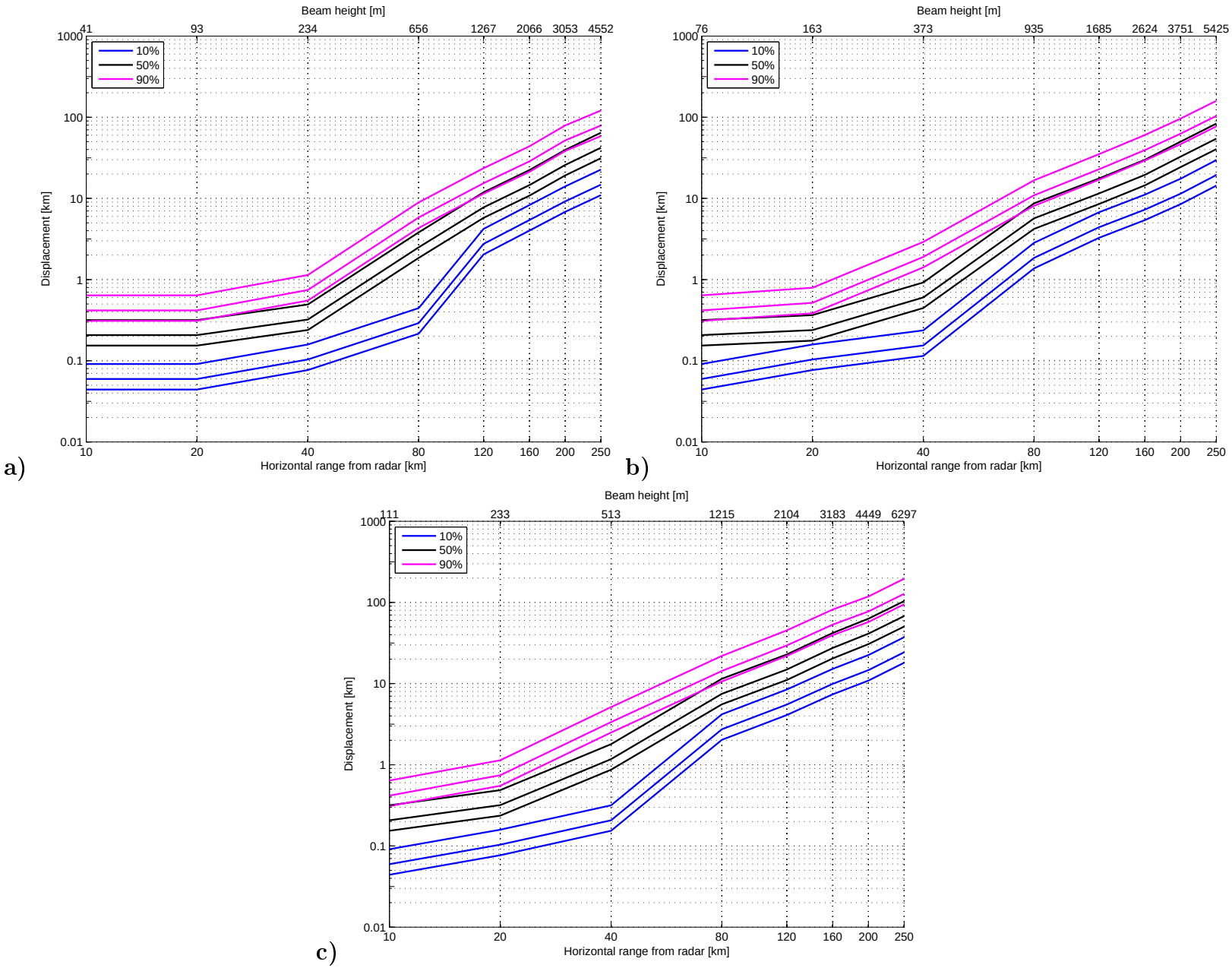

Table A.1 *Wind drift displacement statistics for rain cases. Figure a) represents elevation of 0.2 degrees, figure b) 0.4 degrees and figure c) 0.6 degrees.*

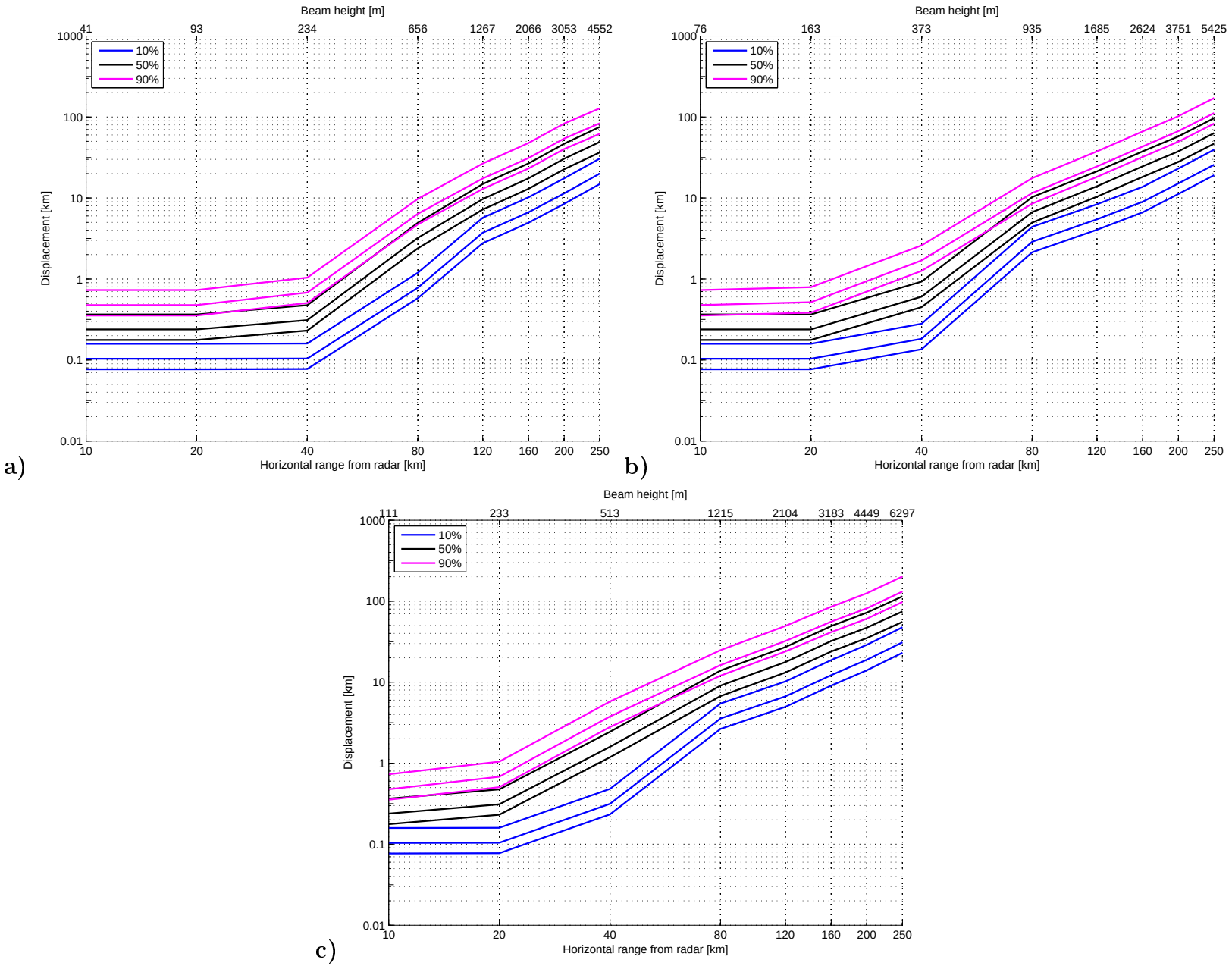

Table A.2 *Wind drift displacement statistics for sleet cases. Figure a) represents elevation of 0.2 degrees, figure b) 0.4 degrees and figure c) 0.6 degrees.*

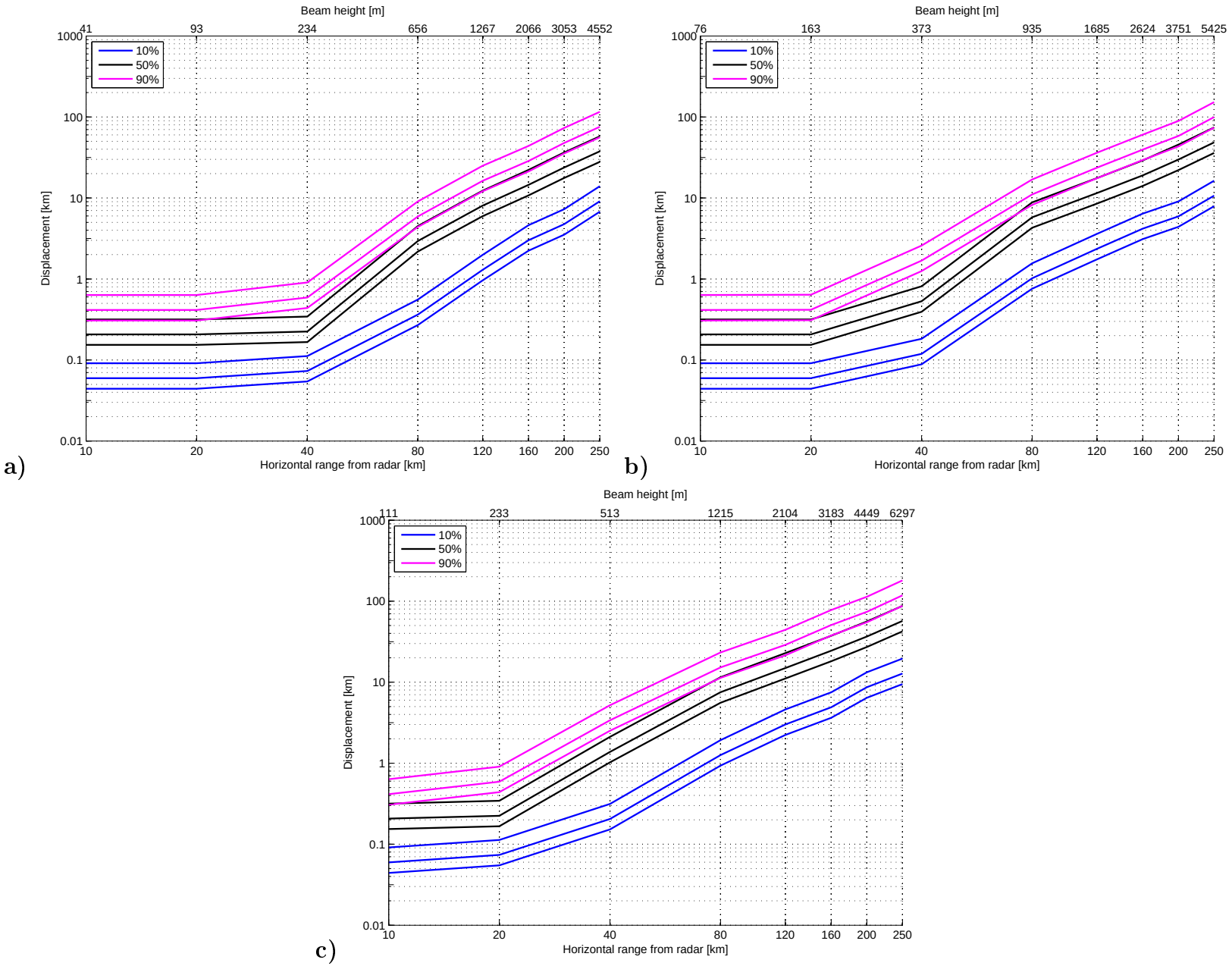

Table A.3 *Wind drift displacement statistics for snow cases. Figure a) represents elevation of 0.2 degrees, figure b) 0.4 degrees and figure c) 0.6 degrees.*

Appendix B

Time series comparisons between trajectory-corrected and uncorrected radar reflectivity

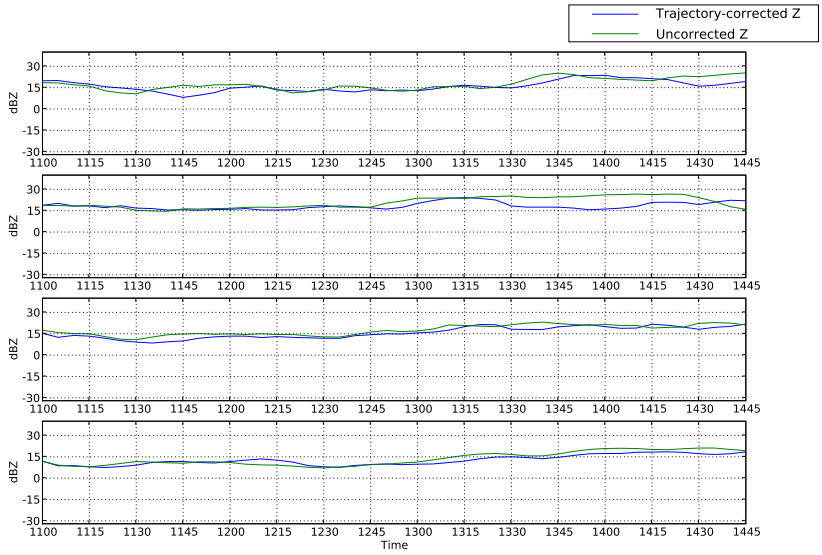

Figure B.1 *Radar reflectivity time series from 23. November 2008. Location distance from radar is 75 kilometers.*

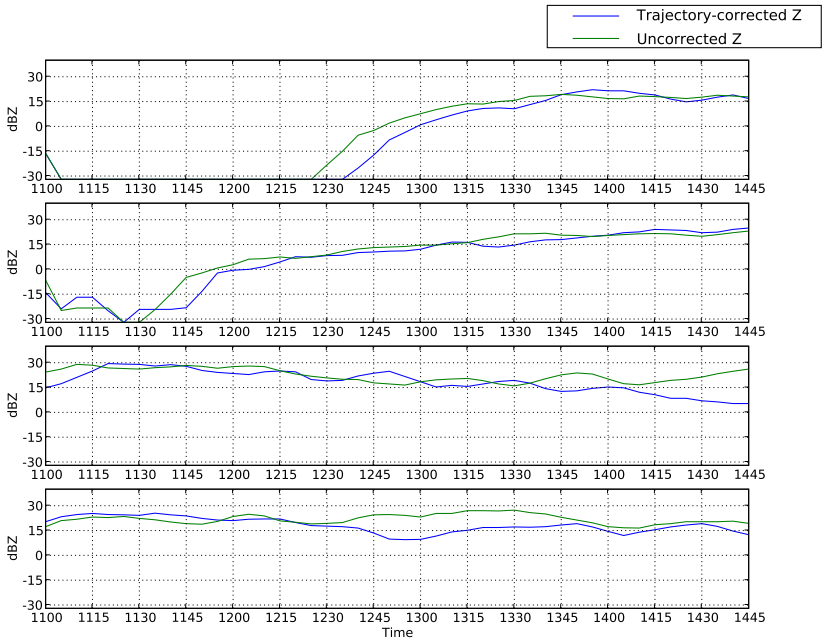

Figure B.2 *Radar reflectivity time series from 30. January 2008. Location distance from radar is 75 kilometers.*

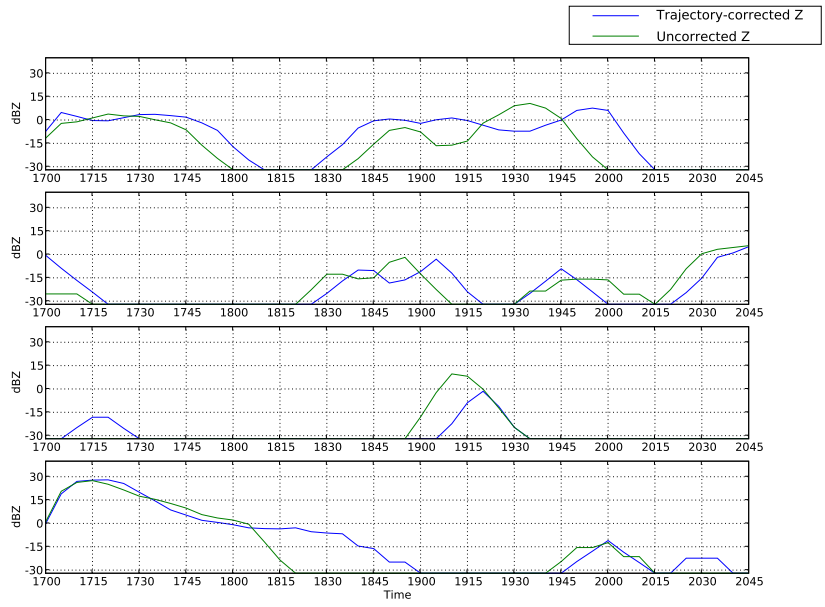

Figure B.3 *Radar reflectivity time series from 23. March 2008. Location distance from radar is 75 kilometers.*